Normalizing Flows for Interventional Density Estimation

Valentyn Melnychuk [1] **Dennis Frauen** [1] **Stefan Feuerriegel** [1]

Abstract

Existing machine learning methods for causal inference usually estimate quantities expressed via the mean of potential outcomes (e.g., average treatment effect). However, such quantities do not capture the full information about the distribution of potential outcomes. In this work, we estimate the *density* of potential outcomes after interventions from observational data. For this, we propose a novel, fully-parametric deep learning method called *Interventional Normalizing Flows*. Specifically, we combine two normalizing flows, namely (i) a nuisance flow for estimating nuisance parameters and (ii) a target flow for parametric estimation of the density of potential outcomes. We further develop a tractable optimization objective based on a one-step bias correction for efficient and doubly robust estimation of the target flow parameters. As a result, our *Interventional Normalizing Flows* offer a properly normalized density estimator. Across various experiments, we demonstrate that our *Interventional Normalizing Flows* are expressive and highly effective, and scale well with both sample size and high-dimensional confounding. To the best of our knowledge, our *Interventional Normalizing Flows* are the first proper fully-parametric, deep learning method for density estimation of potential outcomes.

1. Introduction

Causal inference increasingly makes use of machine learning methods to estimate treatment effects from observational data (e.g., van der Laan et al., 2011; Künzel et al., 2019; Curth & van der Schaar, 2021; Kennedy, 2022). This is relevant for various fields including medicine (e.g., Bica et al., 2021), marketing (e.g., Yang et al., 2020), and policy-making (e.g., Hünermund et al., 2021). Here, causal inference from observational data promises great value, especially when experiments for determining treatment effects are costly or even unethical.

The vast majority of the machine learning methods for causal inference estimate *averaged* quantities expressed by the (conditional) mean of potential outcomes. Examples of such quantities are the average treatment effect (ATE) (e.g., Shi et al., 2019; Hatt & Feuerriegel, 2021), the conditional average treatment effect (CATE) (e.g., Shalit et al., 2017; Hassanpour & Greiner, 2019; Zhang et al., 2020), and treatment-response curves (e.g., Bica et al., 2020; Nie et al., 2021). Importantly, these estimates only describe averages *without* distributional properties.

However, making decisions based on averaged causal quantities can be misleading and, in some applications, even dangerous (Spiegelhalter, 2017; van der Bles et al., 2019). On the one hand, if potential outcomes have different variances or number of modes, relying on the average quantities provides incomplete information about potential outcomes, and may inadvertently lead to local – and not global – optima during decision-making. On the other hand, distributional knowledge is needed to account for uncertainty in potential outcomes and thus informs how likely a certain outcome is. For example, in medicine, knowing the distribution of potential outcomes is highly important (Gische & Voelkle, 2021): it gives the probability that the potential outcome lies in a desired range, and thus defines the probability of treatment success or failure.[1] Motivated by this, we aim to estimate the ***density*** of potential outcomes.

An example highlighting the need for estimating the ***density*** of potential outcomes is shown in Fig. 1. Here, we simulated outcomes according to a given structural causal model (SCM). The potential outcomes $Y[a]$ can be sampled by setting the binary treatment to a specific value in the equation

[1]LMU Munich & Munich Center for Machine Learning (MCML), Munich, Germany. Correspondence to: Valentyn Melnychuk <melnychuk@lmu.de>.

Proceedings of the 40th International Conference on Machine Learning, Honolulu, Hawaii, USA. PMLR 202, 2023. Copyright 2023 by the author(s).

[1]For example, patients with prediabetes are oftentimes treated with metformin monotherapy, which reduces blood glucose sugar (HbA1c) by an *average* of 1.1% (95% confidence interval: 0.9 to 1.3%) (Hirst et al., 2012). Yet, there is often large *skewness* in the potential outcome. While metformin monotherapy is highly effective for some individuals, it fails to achieve glycemic targets for 50% of the patients (Shin, 2019). Here, it is indicated that a second-line anti-diabetes drug is prescribed. Crucially, standard confidence intervals cannot disclose that metformin is harmful to some patients while densities can.

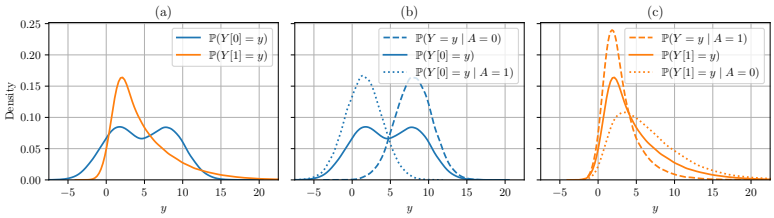

$$X := U_X; \quad U_X \sim \text{Mixture}(0.5N(0,1) + 0.5N(b,1))$$

$$\pi(x) = \frac{N(X;0,1)}{N(X;0,1) + N(X;b,1)}$$

$$A := \begin{cases} 1, & -U_A < \log\left(\pi(x)/(1-\pi(x))\right) \\ 0, & \text{otherwise} \end{cases}; U_A \sim \text{Logistic}(0,1)$$

$$Y := U_Y + \begin{cases} X^2 - 1.82X + 2, & A = 1 \\ 2.18X + 1.5, & A = 0 \end{cases}; \quad U_Y \sim N(0,1)$$

Figure 1. Motivating example showing the densities of observational, interventional, and counterfactual distributions of outcome Y. These are simulated via the structural causal model on the right (here: $N(x; \mu, \sigma^2)$ are densities of the normal distribution; and $b = 3$ is a covariates shift, which regulates the probability of treatment assignment). Potential outcomes have different distributions but the same mean $\mathbb{E}(Y[0]) = \mathbb{E}(Y[1]) \approx 4.77$ and the same variance $\text{var}(Y[0]) = \text{var}(Y[1]) \approx 4.06$. Here, $Y[a]$ is the potential outcome given treatment a. **(a)** Interventional distributions. **(b)** and **(c)** Observational and counterfactual distributions for the same outcomes. As shown here, the observational, interventional, and counterfactual distributions can be substantially different.

for Y (cf. Appendix B). At the same time, by filtering for only the (un)treated population and applying the same equation with a counterfactual treatment, we obtain counterfactual outcomes $Y[a] \mid A = a'$. We observe that the potential outcomes have the same mean (i.e., $\mathbb{E}(Y[0]) = \mathbb{E}(Y[1])$) and the same variance (i.e., $\text{var}(Y[0]) = \text{var}(Y[1])$). Hence, the ground-truth ATE equals zero. Nevertheless, the distributions of potential outcomes (i. e., $\mathbb{P}(Y[a])$) are clearly different. Hence, in medical practice, acting upon the ATE without knowledge of the distributions of potential outcomes could have severe, negative effects. To show this, let us consider a "do nothing" treatment ($a = 0$) and some medical treatment ($a = 1$). Further, let us consider an outcome to be successful if some risk score Y is below the threshold of five. Then, the probability of treatment success (i. e., $\mathbb{P}(Y[1] < 5.0) \approx 0.63$) is much larger than the probability of success after the "do nothing" treatment (i. e., $\mathbb{P}(Y[0] < 5.0) \approx 0.51$), highlighting the importance of treatment.

In this paper, we aim to estimate the ***density*** of potential outcomes after intervention a, i. e., $\mathbb{P}(Y[a] = y)$. From this point on, we refer to this task as ***interventional density estimation*** (IDE). Estimating the density of interventions has several crucial advantages: it allows to identify multi-modalities in the distribution of potential outcomes; it allows to estimate quantiles of the distribution; and it allows to compute the probability with which a potential outcome lies in a certain range. Importantly, traditional density estimation methods are **not** applicable for IDE due to the fundamental problem of causal inference: that is, the counterfactual outcomes are typically never observed, and, hence, the sample from ground-truth interventional distribution is also inaccessible. Efficient IDE is also significantly more challenging than an efficient estimation of the averaged causal quantities. The reason is that density is a functional, infinitely-dimensional target estimand, and, hence, standard efficiency theory is **not** applicable.

Existing literature offers either *semi- or non-parametric* methods for IDE.[2] Examples are kernel density estimation (Kim et al., 2018) and kernel mean embeddings of distributions (Muandet et al., 2021). However, both methods have a crucial limitation: estimated densities could be unnormalized or even return negative values (which, by definition, is not possible). Furthermore, both methods neither scale well with the sample size nor with the dimensionality of covariates. As a remedy, Kennedy et al. (2023) introduced a theory for efficient *semi-parametric* IDE estimation, rendering fully-parametric modeling possible. However, the authors did not provide a proper, flexible instantiation of the theory: the solutions proposed in (Kennedy et al., 2023) are either (i) non-universal (e. g., limited to the exponential family) or (ii) not proper density estimators (e. g., the truncated series estimator).

Here, we propose a *proper fully-parametric* method. Different from semi- and non-parametric methods, our fully-parametric method has several practical advantages: it automatically provides properly normalized density estimators, it allows one to sample from the estimated density, and it generally scales well with large and high-dimensional datasets. However, to the best of our knowledge, there is no fully-parametric, deep learning method for IDE. To achieve this, we later make a non-trivial extension of the theoretical results for semi-parametric IDE estimation from (Kennedy et al., 2023) adopted to fully-parametric IDE estimation.

In this paper, we develop a novel, fully-parametric deep learning method: ***Interventional Normalizing Flows*** (INFs). Our INFs build upon normalizing flows (NFs) (Tabak & Vanden-Eijnden, 2010; Rezende & Mohamed, 2015), but which we carefully adapt for causal inference. This requires several non-trivial adaptations. Specifically, we combine two NFs: a (i) nuisance flow for estimating nuisance parameters, and a (ii) target flow for a parametric estimation of the density of potential outcomes. Here, we construct a novel, tractable optimization objective based on a one-step bias correction to allow for efficient and doubly robust estima-

[2]We distinguish the interventional distribution (i.e., $\mathbb{P}(Y[a])$) and the counterfactual distribution (i.e., $\mathbb{P}(Y[a] \mid A = a')$), which are different in general. This can be seen by comparing plots (a) vs. (b) and (c) in Fig. 1. For further information, we refer to Appendix B.

Table 1. Overview of methods for interventional density estimation from observational data.

Method	Parametric	Estimator type	Efficiency wrt.	Base density model	Proper density	Universal
Kim et al. (2018)	semi-parametric	A-IPTW	L_1 distance	kernel density estimation (KDE)	✗	✓
Muandet et al. (2021)	non-parametric	plug-in	—	distributional kernel mean embeddings (DKME)	✗	✓
Kennedy et al. (2023)	semi- / fully-parametric	A-IPTW	moment condition	exponential family	✓	✗
				truncated series (TS)	✗	✓
INFs (this paper)	fully-parametric	A-IPTW	moment condition	normalizing flows (NFs)	✓	✓

A-IPTW: augmented inverse propensity of treatment weighted

tion. In the end, we develop a two-step training procedure to train both the nuisance and the target flows.

Overall, our **main contributions** are following:[3]

1. We introduce the first proper fully-parametric, deep learning method for interventional density estimation, called *Interventional Normalizing Flows* (INFs). Our INFs provide a properly normalized density estimator.
2. We extend the results of (Kennedy et al., 2023) and derive a tractable optimization problem with a one-step bias correction for efficient and doubly robust estimation. This allows for an effective two-step training procedure with our INFs.
3. We demonstrate in various experiments that our INFs are highly expressive and effective. A major advantage owed to the parametric form of the target flow is that our INFs scale well to both large and high-dimensional datasets in comparison to other non- and semi-parametric methods.

2. Related work

Recently, there has been a great interest in using machine learning and, specifically, deep learning for estimating causal quantities. Examples are machine learning for estimating ATE (e.g., Shi et al., 2019; Hatt & Feuerriegel, 2021), CATE (e.g., Johansson et al., 2016; Alaa & van der Schaar, 2018; Wager & Athey, 2018; Curth & van der Schaar, 2021; Hatt et al., 2022; Kuzmanovic et al., 2023), and treatment-response curves (e.g., Bica et al., 2020; Schwab et al., 2020; Nie et al., 2021; Schweisthal et al., 2023). In this regard, some papers proposed uncertainty-aware methods, e. g., by using the variance of potential outcomes (Alaa & van der Schaar, 2017; Jesson et al., 2020), or the conditional outcome distribution (Jesson et al., 2021; 2022). However, the aforementioned works are all concerned with estimating *averaged* causal quantities expressed via the mean of potential outcomes or *epistemic uncertainty* around these quantities.[4] In contrast, we aim to estimate the *density* of outcomes after the intervention, i. e., the *aleatoric* uncertainty of the potential outcomes (=uncertainty due to the data-generating process at the population level).

2.1. Interventional density estimation

Table 1 lists existing methods for IDE. Importantly, these are either **non-parametric** or **semi-parametric**. Kim et al. (2018) developed a doubly robust kernel density estimation (KDE) with functional regressions. Muandet et al. (2021) proposed kernel mean embeddings of distributions (DKME), which provides a non-parametric plug-in estimator. However, both methods (Kim et al., 2018; Muandet et al., 2021) have limitations. (1) They do not provide a properly normalized density estimator. Hence, the estimated densities can be unnormalized or even negative, yet which, by definition, is not possible. (2) They do not offer direct sampling, which would allow one to sample from the estimated density without an additional algorithm. This may complicate computations of the test log-probability or empirical Wasserstein distance during evaluation. (3) Another limitation of both non-parametric and semi-parametric methods is that they typically scale not well. This is unlike **fully-parametric** methods, which scale well to both large and high-dimensional datasets.

Kennedy et al. (2023) introduced a theory for efficient semi-parametric IDE, which also extends to fully-parametric estimation. The authors proposed a hypothetical estimator as a solution to a multivariate system of integral equations, namely a bias-corrected moment condition (see Eq. 19 therein). However, the theory comes *without* an algorithmic instantiation in the form of a proper universal density estimator: the proposed solutions are either (i) non-universal or (ii) not proper density estimators. By (i), we refer to the exponential family, as it requires a very strong assumption about the data and is not universal.[5] By (ii), we refer to the truncated series, which are not a proper density estimator in the sense that the estimated density could have negative values and is only normalized in a *bounded region* of the outcome space (Efromovich, 2010). Therefore, they would be a particularly bad model for the distributions with heavy tails and multiple low-density regions. Also, truncated se-

[3] Code is available at https://github.com/Valentyn1997/INFs.

[4] Jesson et al. (2020; 2021) considered *epistemic* uncertainty of CATE estimation (=uncertainty due to estimation) and uncertainty due to violations of causal assumptions (e. g., positivity or exchangeability).

[5] Although, more flexible extensions of exponential families exist, e. g., (Ranganath et al., 2015), they contain an intractable normalization constant and thus are not proper estimators.

ries estimators do not scale well beyond one-dimensional distributions (Gellerstedt & Sjölin, 2022). For example, large amounts of training data are required to sufficiently outnumber the degrees of freedom of the model.

The methods for IDE above (Kim et al., 2018; Muandet et al., 2021; Kennedy et al., 2023) build upon standard assumptions for causal identifiability via back-door adjustment.[6] We later adopt the *same* assumptions for IDE (see Section 3), and we then develop a fully-parametric, deep learning method called INFs. As one of our contributions, we adopt the theoretical framework of Kennedy et al. (2023) and convert the bias-corrected moment condition into a tractable optimization objective, for which we then show how to solve it effectively with deep learning. Our method has three favorable properties: it yields a proper density estimator, it allows for direct sampling, and it scales well.

2.2. Efficient estimation

In the context of treatment effect estimation, the so-called augmented inverse propensity of treatment weighted (A-IPTW) estimators were developed for efficient, semi-parametric estimation of *finitely-dimensional target estimands* (parameters) (Robins, 2000). Formally, A-IPTW estimation performs a first-order bias correction of plug-in models (Bickel et al., 1993; Chernozhukov et al., 2018). A-IPTW estimation also offers the property of being double robust, i. e., fast convergence rates even if one of the nuisance parameter estimators converges slowly (Kennedy, 2020).

Our task is different from the above: interventional density is a *functional, infinitely-dimensional target estimand*, because of which the standard efficiency theory does not apply here. As a remedy, Kennedy et al. (2023) proposed to estimate finitely-dimensional projection parameters and then formulated a semi-parametric estimation as a solution to the bias-corrected moment condition. Nevertheless, no flexible algorithmic instantiation in the form of a proper universal density estimator has been implemented so far. Later, we make a non-trivial extension to derive a tractable optimization problem for our INFs.

2.3. Normalizing flows

Normalizing flows were introduced for expressive variational approximations in variational autoencoders (Tabak & Vanden-Eijnden, 2010; Rezende & Mohamed, 2015). We provide a background on NFs in Appendix B. One practical benefit of NFs is that they yield universal density approximators (Dinh et al., 2014; 2017; Huang et al., 2018; Durkan et al., 2019). Furthermore, NFs can be leveraged for conditional density estimation (e. g., via so-called hypernetworks (Trippe & Turner, 2018)). NFs were previously used for causal inference, but in a different setting from ours (see Appendix A).

Research gap: Existing methods for IDE are either *non- or semi-parametric*. To the best of our knowledge, our work is the first to propose a *fully-parametric*, deep learning method for IDE.

3. Setup: Interventional density estimation

Notation. Let $\mathbb{P}(Z)$ be a distribution of a random variable Z, and let $\mathbb{P}(Z = z)$ be its density or probability mass function. Let $\pi_a(x) = \mathbb{P}(A = a \mid X = x)$ denote the propensity score. Further, $\mathbb{1}(\cdot)$ is the indicator function; $\mathbb{P}_n\{f(X)\} = \frac{1}{n}\sum_{i=1}^{n} f(X_i)$ is the sample average of a random $f(X)$; and $\mathbb{P}_b^{\mathcal{B}}\{f(X)\}$ is the average evaluated on a minibatch $\mathcal{B}$ of size b. For readability, we sometimes highlight random variables and the corresponding averaging operator in green color. Furthermore, $\mathbb{P}(Y \mid X, A)$ is the conditional distribution of the outcome Y.

Problem statement. In this work, we aim at estimating the ***interventional density*** from observational data, namely $\hat{\mathbb{P}}(Y[a] = y)$. To compare the goodness-of-fit of different estimators, we evaluate the distributional distance between the ground-truth interventional density and the estimated density. Such distributional distances include, e.g., the average log-probability and the empirical Wasserstein distance.

We build upon the standard setting of potential outcomes framework (Rubin, 1974), where $Y[a]$ stands for the potential outcome after intervening on treatment by setting it to a. That is, we consider an observational sample $\mathcal{D}$ with d_X-dimensional covariates $X \in \mathcal{X} \subseteq \mathbb{R}^{d_X}$, a treatment $A \in \{0, 1\}$, and a d_Y-dimensional continuous outcome $Y \in \mathcal{Y} \subseteq \mathbb{R}^{d_Y}$, drawn i.i.d. We consider $d_Y = 1$ if not stated explicitly. We assume the treatment to be binary, but note that our INFs also work with categorical treatments. We denote $\mathcal{D} = \{X_i, A_i, Y_i\}_{i=1}^{n} \sim \mathbb{P}(X, A, Y)$, where n is the sample size, and i is the index of an observation. For example, in critical care, the patient covariates X are different risk factors (e.g., age, gender, weight, prior diseases), the treatment is whether a ventilator is applied, and the outcome is the probability of patient survival. The covariates X are also called confounders if $\mathbb{P}(Y[a]) \neq \mathbb{P}(Y \mid A = a)$.

Identifiability. To identify the interventional density, we make the following identifiability assumptions with respect to the data-generating mechanism of $\mathcal{D}$: (1) *Positivity:* For some $\epsilon > 0$, $\mathbb{P}(1 - \epsilon \geq \pi_a(X) \geq \epsilon) = 1$. (2) *Consistency:* If $A = a$ for some patient, then $Y = Y[a]$. (3) *Exchangeability:* $A \perp\!\!\!\perp Y[a] \mid X$ for all a. Note that these assumptions are standard in the literature (Kim et al., 2018; Muan-

[6] A recent work by Bhattacharyya et al. (2022) develops IDE for any identifiable interventional distribution in an arbitrary causal Bayesian network, but only for discrete variables.

det et al., 2021; Kennedy et al., 2023). Under assumptions (1)–(3), the density of interventional distribution $\mathbb{P}(Y[a])$ can be expressed in terms of observational distribution with back-door adjustment, i.e.,

$$\mathbb{P}(Y[a]=y) = \mathop{\mathbb{E}}_{X\sim\mathbb{P}(X)}\big(\mathbb{P}(Y=y \mid X, A=a)\big), \tag{1}$$

where $\mathbb{P}(Y=y \mid X, A)$ is the conditional density of the outcome. For more details on the potential outcomes framework and identifiability, we refer to Appendix B.

Plug-in estimator. A straightforward approach for IDE (Robins & Rotnitzky, 2001) is the following: first, one estimates the conditional outcome distribution, $\hat{\mathbb{P}}(Y \mid X, A)$ (here, any method for conditional density estimation could be used). Then, one takes a sample average over covariates X:

$$\hat{\mathbb{P}}^{\text{PI}}(Y[a]=y) = \mathbb{P}_n\{\hat{\mathbb{P}}(Y=y \mid X, A=a)\}. \tag{2}$$

This estimator is an unbiased but inefficient estimator of interventional density, which is known as *semi-parametric plug-in estimator*. Semi-parametric IDE, unlike, e. g., semi-parametric ATE estimation, is highly problematic. For large sample sizes, the semi-parametric estimator requires averaging over the full sample for each evaluation point. Motivated by this, we aim to develop a proper fully-parametric estimator.

4. Theoretical background for fully-parametric IDE

In this section, we introduce a theory for fully-parametric estimation of interventional density. First, we provide a theoretic background, as introduced in (Kennedy et al., 2023). Here, we describe a projection parameter as a solution to the moment condition and then we list two estimators, i. e., *covariate-adjusted (CA) estimator* and efficient *augmented inverse propensity of treatment weighted (A-IPTW) estimator*. Second, we elaborate on the A-IPTW estimator and translate it into an optimization objective, which constitutes one of our contributions.

We start by defining a parametric model, $\{g(y;\beta_a) \mid \beta_a \in \mathbb{R}^d\}$, where $\beta_a \in \mathbb{R}^d$ are parameters of estimator, and $g(\cdot;\beta_a)$ is a density, i. e., $\int_{y\in\mathcal{Y}} g(y;\beta_a)\,\mathrm{d}y = 1$. For IDE, we approximate the interventional distribution $\mathbb{P}(Y[a])$ with a distribution from our parametric model. We aim at minimizing the distributional distance (specifically KL-divergence) between $\mathbb{P}(Y[a])$ and $g(\cdot;\beta_a)$ via

$$\begin{aligned}\hat{\beta}_a &= \arg\min_{\beta_a} \mathrm{KL}\left(\mathbb{P}(Y[a]) \,\middle\|\, g(\cdot;\beta_a)\right)\\ &= \arg\min_{\beta_a} \mathop{\mathbb{E}}_{Y^a\sim\mathbb{P}(Y[a])}\big(-\log g(Y^a;\beta_a)\big),\end{aligned} \tag{3}$$

where $\hat{\beta}_a$ are called *projection parameters* as they project the true interventional density onto a class $\{g(\cdot;\beta_a); \beta_a \in \mathbb{R}^d\}$.

4.1. Projection parameters as solution to moment condition (Kennedy et al., 2023)

Covariate-adjusted estimator. Let the d-dimensional random variable $T(Y;\beta_a) = -\nabla_{\beta_a}\log g(Y;\beta_a)$ denote the score function. Following Kennedy et al. (2023), the projection parameters can be equivalently expressed under mild conditions[7] as a solution to the *moment condition* $m(\beta_a) \overset{!}{=} 0$, where

$$\begin{aligned}m(\beta_a) &= \mathop{\mathbb{E}}_{Y^a\sim\mathbb{P}(Y[a])} T(Y^a;\beta_a)\\ &= \mathop{\mathbb{E}}_{X\sim\mathbb{P}(X)}\Big(\mathbb{E}\big(T(Y;\beta_a) \mid X, A=a\big)\Big).\end{aligned} \tag{4}$$

Here, the moment condition is the expected score function of the potential outcome. Throughout the paper, we assume that the moment condition has a unique solution, and, therefore, the minimization task in Eq. (3) and the root-finding task in Eq. (4) are equivalent.

In practice, we have neither observations from the interventional distribution nor counterfactual outcomes. Therefore, we cannot use the ground-truth $\mathbb{P}(Y[a])$ but, instead, must use the plug-in estimator distribution from Eq. (2). Specifically, we can obtain a plug-in estimator of projection parameters, i. e., $\hat{\beta}_a^{\text{PI}}$, either by minimizing a cross-entropy loss or by solving the moment condition, both of which are equivalent:

$$\begin{aligned}&\hat{\beta}_a^{\text{PI}} = \arg\min_{\beta_a} \mathop{\mathbb{E}}_{\hat{Y}^a\sim\mathbb{P}_n\{\hat{\mathbb{P}}(Y\mid X, A=a)\}} -\log g(\hat{Y}^a;\beta_a)\\ \iff &\hat{m}^{\text{PI}}(\beta_a) = \mathop{\mathbb{E}}_{\hat{Y}^a\sim\mathbb{P}_n\{\hat{\mathbb{P}}(Y\mid X, A=a)\}} T(\hat{Y}^a;\beta_a) \overset{!}{=} 0.\end{aligned} \tag{5}$$

Then, we can define a *parametric covariate-adjusted* (CA) estimator as $\hat{\mathbb{P}}^{\text{CA}}(Y[a]=y) = g(y;\hat{\beta}_a^{\text{PI}})$. By choosing a sufficiently expressive class of densities for both g and the conditional density estimator $\hat{\mathbb{P}}(Y \mid X, A)$ (e. g., normalizing flows), CA can be shown to consistently estimate the interventional density (see Appendix B.5 in Kennedy et al. (2023)).

Augmented inverse propensity of treatment weighted estimator. In the following, we aim to develop an efficient estimator of the projection parameter $\hat{\beta}_a$ from Eq. (3) or, equivalently, the moment condition $\hat{m}(\beta_a)$ at fixed β_a from Eq. (4). For this, we make use of semi-parametric efficiency theory (van der Laan & Robins, 2003; Kennedy et al., 2023). We provide a background on efficiency theory in Appendix B.

Kennedy (2022) showed that the efficient influence function

[7] We assume that $g(\cdot,\beta_a)$ is differentiable in β_a and that the minimizer of Eq. (3) is unique.

$\phi_a(T, \mathbb{P})$ for the functional $\mathbb{E}(\mathbb{E}(T \mid X, A = a))$ equals to

$$\phi_a(T; \mathbb{P}) = \frac{\mathbb{1}(A = a)}{\pi_a(X)} \Big(T - \mathbb{E}(T \mid X, A = a)\Big) + \mathbb{E}(T \mid X, A = a) - \mathop{\mathbb{E}}_{X \sim \mathbb{P}(X)} (\mathbb{E}(T \mid X, A = a)). \tag{6}$$

Here, we use red color to show the nuisance parameters of $\mathbb{P}$ that are influencing the functional. We emphasize that the nuisance parameters (i. e., the propensity score and conditional expectations/probabilities) can be either known or estimated.

The efficient influence function in Eq. (6) allows us to construct an efficient estimator of the moment condition. Following (Kennedy et al., 2023), we transform the plug-in estimator $\hat{m}^{\text{PI}}(\beta_a)$ from Eq. (5) into an efficient estimator with the help of a *one-step bias correction*. In our case, the bias-corrected moment condition has the following form:

$$\hat{m}^{\text{A-IPTW}}(\beta_a) = \hat{m}^{\text{PI}}(\beta_a) + \mathbb{P}_n\big\{\phi_a(T(Y; \beta_a); \hat{\mathbb{P}})\big\} \stackrel{!}{=} 0, \tag{7}$$

where $\hat{\mathbb{P}} = \{\hat{\pi}_a(x), \hat{\mathbb{P}}(Y \mid X, A)\}$ are the estimated nuisance parameters of $\mathbb{P}$. We call the solution of the bias-corrected moment equation $\hat{\beta}_a^{\text{A-IPTW}}$ an *augmented inverse propensity of treatment weighted* (A-IPTW) estimator of the projection parameters. Then, estimated interventional density is $\hat{\mathbb{P}}^{\text{A-IPTW}}(Y[a] = y) = g(y; \hat{\beta}_a^{\text{A-IPTW}})$.

4.2. Projection parameters as a solution to optimization objective

Previously, Kennedy et al. (2023) proposed to directly solve the bias-corrected moment condition, i. e., a system of non-linear equations, yet which is generally much harder to solve computationally. In contrast, we develop an optimization objective that can be directly incorporated into a loss of a deep learning density estimator. For that, we transform the bias-corrected moment condition into the following tractable optimization task (see Appendix C for all details).

We first note that the plug-in estimator of moment condition $\hat{m}^{\text{PI}}(\beta_a)$ can be rewritten as

$$\hat{m}^{\text{PI}}(\beta_a) = \mathop{\mathbb{E}}_{\hat{Y}^a \sim \mathbb{P}_n\{\hat{\mathbb{P}}(Y \mid X, A=a)\}} T(\hat{Y}^a; \beta_a) \tag{8}$$

$$= \int_{\mathcal{Y}} T(y; \beta_a)\, \mathbb{P}_n\{\hat{\mathbb{P}}(Y = y \mid X, A = a)\}\, \mathrm{d}y \tag{9}$$

$$= \mathbb{P}_n\Big\{\hat{\mathbb{E}}\big(T(Y; \beta_a) \mid X, A = a\big)\Big\}, \tag{10}$$

where the last equality follows from the definition of the conditional expectation. Then, we notice that the last term of the influence function, $\mathop{\mathbb{E}}_{X \sim \mathbb{P}(X)} (\mathbb{E}(T \mid X, A = a))$, is, in fact, non-random and could be brought out from the sample average in Eq. 7. Furthermore, after switching from $\mathbb{P}$ to $\hat{\mathbb{P}}$, this term exactly coincides with $\hat{m}^{\text{PI}}(\beta_a)$, so that the one-step bias-corrected equation is simplified to

$$\hat{m}^{\text{A-IPTW}}(\beta_a) = \mathop{\mathbb{E}}_{\hat{Y}^a \sim \mathbb{P}_n\{\hat{\mathbb{P}}(Y \mid X, A=a)\}} T(\hat{Y}^a; \beta_a) \tag{11}$$

$$+ \mathbb{P}_n\left\{\frac{\mathbb{1}(A = a)}{\hat{\pi}_a(X)} \Big(T(Y; \beta_a) - \mathop{\mathbb{E}}_{Y \sim \hat{\mathbb{P}}(Y \mid X, A=a)} T(Y; \beta_a)\Big)\right\}. \tag{12}$$

After taking the antiderivative with respect to β_a, we yield the following optimization objective

$$\hat{\beta}_a^{\text{A-IPTW}} = \arg\min_{\beta_a} \Bigg[\underbrace{\mathop{\mathbb{E}}_{\hat{Y}^a \sim \mathbb{P}_n\{\hat{\mathbb{P}}(Y \mid X, A=a)\}} \Big(- \log g(\hat{Y}^a; \beta_a)\Big)}_{\text{cross-entropy loss}} \tag{13}$$

$$\underbrace{- \mathbb{P}_n\left\{\frac{\mathbb{1}(A = a)}{\hat{\pi}_a(X)} \Big(\log g(Y; \beta_a) - \mathop{\mathbb{E}}_{Y \sim \hat{\mathbb{P}}(Y \mid X, A=a)} \big(\log g(Y; \beta_a)\big)\Big)\right\}}_{\text{one-step bias correction}} \Bigg].$$

Unlike the plug-in estimator ($\hat{\beta}_a^{\text{PI}}$), the A-IPTW estimator achieves efficiency and possesses a double robustness property. Here, formally speaking, we still mean efficiency with respect to the moment condition, i. e. $m(\beta_a)$. This way of defining efficiency is particularly useful when the solution to the moment condition in Eq. (4) is non-unique, e. g., due to the usage of parametric deep learning models. In this case, we can informally define the so-called efficient estimation of the projection parameters with respect to the equivalence class. All the parameters $\hat{\beta}_a^{\text{A-IPTW}}$, which fall into this class, will satisfy the efficiently estimated moment condition, Eq. (7).

5. Interventional Normalizing Flows

In the following, we describe our *Interventional Normalizing Flows*: a proper fully-parametric method for interventional density estimation via deep learning. First, we describe all the components of our architecture and, then, introduce an efficient estimation using one-step bias correction.

5.1. Components

In our INFs, we combine two normalizing flows, which we refer to as (i) *nuisance flow* and (ii) *target flow* (see Fig. 2). The rationale for this is based on our derivations in Section 3, according to which a fully-parametric IDE requires two models: (i) one for the estimation of nuisance parameters, and (ii) one for the subsequent optimization of the learning objective with respect to projection parameters. Accordingly, both NFs in our INFs have thus different objectives: (i) the nuisance flow estimates the nuisance parameters (i.e., the propensity score and the conditional outcome distribution); and (ii) the target flow uses the estimated nuisance parameters to estimate the projection parameters.

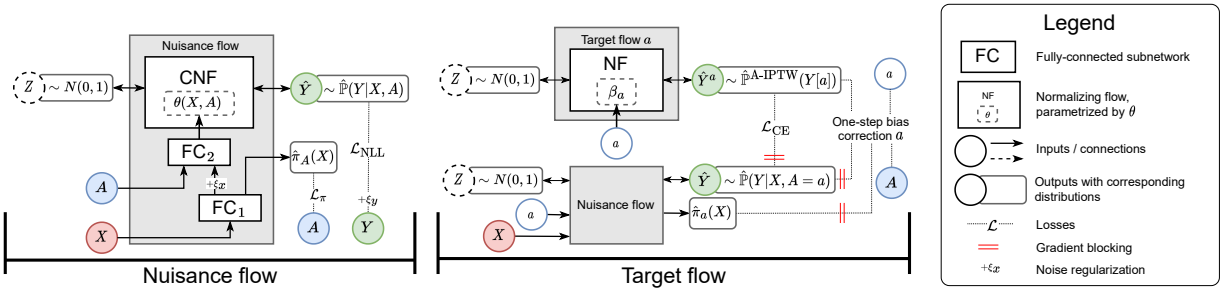

Figure 2. Overview of *Interventional Normalizing Flows*. Our INFs combine two normalizing flows, which we call "nuisance flow" and "target flow". The nuisance flow estimates the nuisance parameters, i.e., the propensity score $\hat{\pi}_a(X)$ and the conditional outcome distribution $\hat{\mathbb{P}}(Y \mid X, A)$. The target flow utilizes them to estimate the projection parameters $\hat{\beta}_a^{\text{A-IPTW}}$.

(i) Nuisance flow. The nuisance flow has three components: two fully-connected (FC) subnetworks and a conditional normalizing flow parameterized by θ. The first FC subnetwork (FC_1) takes the covariates X as input and, then, outputs a representation $R \in \mathbb{R}^{d_R}$ together with a propensity score $\hat{\pi}_a(X)$. The second FC subnetwork (FC_2) takes the representation R and the observed treatment A_i as input and, then, outputs the parameters of flow, conditioned on X and A, i. e., $\theta(X, A)$. Together, FC_1 and FC_2 form a so-called hypernetwork (Ha et al., 2017) for the conditional normalizing flow, which allows us to learn the conditional outcome distribution via back-propagation.

Let $\mathcal{L}_{\mathrm{N}}$ be the loss of the nuisance flow. Here, we combine a conditional negative log-likelihood ($\mathcal{L}_{\mathrm{NLL}}$) and binary cross-entropy loss for the propensity score ($\mathcal{L}_\pi$), i.e., $\mathcal{L}_{\mathrm{N}}(\hat{\mathbb{P}}, \hat{\pi}_a) = \mathbb{P}_n\{\mathcal{L}_{\mathrm{NLL}} + \alpha \mathcal{L}_\pi\}$ with $\mathcal{L}_{\mathrm{NLL}} = -\log \hat{\mathbb{P}}(Y = Y \mid X, A)$; $\mathcal{L}_\pi = \mathrm{BCE}(\hat{\pi}_A(X), A)$, where $\alpha > 0$ is a hyperparameter. In general, conditional normalizing flows are prone to overfitting when trained via a conditional negative log-likelihood. To address this, we later employ noise regularization (Rothfuss et al., 2019) in the conditional density estimation.

(ii) Target flow. The target flow uses the outputs of the nuisance flow and then learns the interventional distribution. We first describe the naïve variant of the target flow without one-step bias correction (we introduce this later in Section 5.2). Different from the conditional normalizing flow in the nuisance flow, the target flow is a non-conditional normalizing flow, parameterized by β_a. Specifically, we consider two separate normalizing flows, that is, one for each potential outcome (i.e., $a = 0$ and $a = 1$, respectively).[8]

To fit the target flow, we must solve the moment condition from Eq. (5) or, equivalently, minimize a cross-entropy loss:

$$\mathcal{L}_{\mathrm{CE}}(\beta_a) = \mathop{\mathbb{E}}_{\hat{Y}^a \sim \mathbb{P}_n\{\hat{\mathbb{P}}(Y|X, A=a)\}} - \log g(\hat{Y}^a; \beta_a) \tag{14}$$
$$= -\int_{y \in \mathcal{Y}} \log g(y; \beta_a) \mathbb{P}_n\{\hat{\mathbb{P}}(Y = y \mid X, A = a)\} \, \mathrm{d}y,$$

[8] One can use a single normalizing flow with a hypernetwork for categorical treatments.

where the later integration is performed numerically with quadrature ($d_Y = 1$) or Monte Carlo ($d_Y > 1$) methods.

5.2. One-step bias correction

To provide an efficient estimation for the parameters of the target flow, we augment the cross-entropy loss (Eq. (14)) with a one-step bias correction. To evaluate the bias correction term, we need to compute a conditional cross-entropy loss:

$$\mathcal{L}_{\mathrm{CCE}}(X; \beta_a) = \mathop{\mathbb{E}}_{Y \sim \hat{\mathbb{P}}(Y|X, A=a)} - \log g(Y; \beta_a),$$
$$= -\int_{y \in \mathcal{Y}} \log g(y; \beta_a) \hat{\mathbb{P}}(Y = y \mid X, A = a) \, \mathrm{d}y.$$

Finally, we obtain the loss of the target flow ($\mathcal{L}_{\mathrm{T}}$), which is now suitable for our A-IPTW estimation from Eq. (13). We thus yield

$$\mathcal{L}_{\mathrm{T}}(\beta_a) = \mathcal{L}_{\mathrm{CE}}(\beta_a) + \mathbb{P}_n\left\{\frac{\mathbb{1}(A = a)}{\hat{\pi}_a(X)}\left(-\log g(Y; \beta_a) - \mathcal{L}_{\mathrm{CCE}}(X; \beta_a)\right)\right\}. \tag{15}$$

5.3. Training and inference

Training. To train both components in our INFs, we make use of a two-step training procedure. Specifically, we first fit the nuisance parameters using the nuisance flow. Then, we freeze the parameters of the nuisance flow and fit the target flow. We additionally employ the exponential moving average (EMA) of the target parameters with a smoothing hyperparameter γ to stabilize the training for small minibatch sizes (Polyak & Juditsky, 1992). We show the full algorithm in Appendix D and further implementation details in Appendix E.

Inference time. One main advantage of our nuisance-target model is that the target flow has constant inference time (e.g., during the evaluation phase). Hence, contrary to state-of-the-art baselines, the inference of our INFs do not depend on the dimensionality of covariates (or representation) and the size of the training data. This is a major advantage over semi-parametric plug-in estimators. For a detailed run-

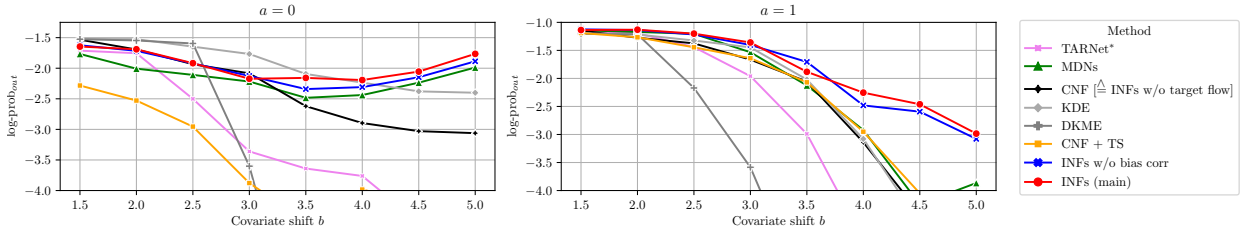

Figure 3. Results for synthetic data based on the SCM from Figure 1. Reported: mean over ten-fold train-test splits. Some runs for MDNs resulted in the log-prob$_{\text{out}} = -\infty$ and, thus, are not shown.

time comparison, we refer to Appendix L. To this end, our method offers great scalability, such as required in medicine.

6. Experiments

To show the effectiveness of our INFs, we use established (semi-)synthetic datasets that have been previously used for treatment effect estimation (Shi et al., 2019; Curth & van der Schaar, 2021). The benefit of (semi-)synthetic datasets is that both factual and counterfactual outcomes are available (i.e., Y_i^{f} and Y_i^{cf}). Therefore, we can obtain a sample from the ground-truth interventional distribution, i. e., $Y[a]_i = \mathbb{1}(A_i = a)\, Y_i^{\text{f}} + \mathbb{1}(A_i \neq a)\, Y_i^{\text{cf}}$, which we can then use for IDE benchmarking.

Evaluation metric. We use the average log-probability as our standard metric for comparing density estimators. It is given by log-prob$_{\mathcal{D}} = \frac{1}{n} \sum_{i=1}^{n} \log \hat{\mathbb{P}}(Y[a] = Y[a]_i)$, where higher values indicate a better fit. The maximum value of the average log-probability is upper-bounded by the entropy, which, in general, is different for each potential outcome. Therefore, we separately report the results for each potential outcome. Of note, the log-probability is equivalent to the empirical KL-divergence.

Baselines. We use state-of-the-art IDE baselines (see Sec. 2.1): (1) an extended TARNet (**TARNet***) (Shalit et al., 2017) estimating the mean of a conditional homoscedastic normal distribution; (2) mixture density networks (**MDNs**) (Bishop, 1994)[9]; (3) conditional normalizing flow (**CNF**) (Trippe & Turner, 2018); (4) kernel density estimation (**KDE**) (Kim et al., 2018); (5) distributional kernel mean embeddings (**DKME**) (Muandet et al., 2021); and (6) truncated series estimator with CNF (**CNF+TS**) as a more flexible baseline from (Kennedy et al., 2023). TARNet*, MDNs, and CNF are semi-parametric plug-in estimators (see Eq. (2)). Importantly, KDE, DKME and CNF+TS do not guarantee a proper density estimation (unlike our INFs). We thus performed an additional re-normalization and negative values clipping, so that we can use the average log-probability as an evaluation metric. Details on the baselines are in Appendix F and on hyperparameter tuning in Appendix G.

[9]MDNs were previously used to estimate the conditional distribution of outcome for quantifying the ignorance regions of CATE estimation (Jesson et al., 2021; 2022). However, this is different from our IDE task.

Ablation studies. We compare three variants of our INFs: (1) **INFs** (main): Our INFs as introduced above using A-IPTW estimation. (2) **INFs w/o target flow**: A simplified variant which uses only the conditional density estimation from the nuisance flow as a semi-parametric plug-in estimator, and thus without target flow. This variant is identical to the CNF baseline. (3) **INFs w/o bias corr**: We use the covariate-adjusted fully-parametric estimator, where the target flow only uses the cross-entropy loss from Eq. (14) but without one-step bias correction. The ablations have the same hyperparameters as our main method for better comparability.

Synthetic data. We generate synthetic data using the SCM ($d_X = 1$) from Fig. 1. Here, we vary the covariate shift b, which controls the overlap between the treated and non-treated population. Notably, low values of b correspond to the case, where both populations are similar or the same, while high values of b result in the violation of the positivity assumption. Further details on the synthetic dataset are in Appendix H. Our INFs achieve clear performance improvements over the baselines, especially for larger b (Fig. 3). Moreover, the ablation studies confirm that our proposed deep learning architecture with one-step bias correction is superior. In Appendix I, we further provide a two-dimensional benchmark, where our INFs again perform best.

IHDP dataset. The Infant Health and Development Program (IHDP) (Hill, 2011) is a semi-synthetic dataset with two synthetic potential outcomes generated from real-world medical covariates ($n = 747, d_X = 25$, see details in Appendix H). Here, we used ten-fold train/test splits (90%/10%) and perform hyperparameter tuning based on the first split. Results are in Table 2. TARNet* is known to entail a ground-truth conditional distribution model and should thus not be interpreted as a baseline but as an upper performance bound. Our INFs reach an equally good performance and, importantly, outperform all the other baselines for both potential outcomes. The ablation study again confirms that our main INFs are superior over the other variants without the target flow and without bias correction. In Appendix J, we repeat the evaluation using the empirical Wasserstein distance with similar findings.

Table 2. Results for IHDP dataset. Reported: mean ± sd.

	$a=0$		$a=1$	
	log-prob$_{\text{in}}$	log-prob$_{\text{out}}$	log-prob$_{\text{in}}$	log-prob$_{\text{out}}$
TARNet* [≙ ground-truth for IHDP]	$\underline{-0.919 \pm 0.011}$	$\mathbf{-0.928 \pm 0.088}$	$\mathbf{-0.635 \pm 0.010}$	$\mathbf{-0.634 \pm 0.075}$
MDNs	-0.927 ± 0.024	-0.942 ± 0.080	-0.679 ± 0.048	-0.684 ± 0.077
CNF [≙ INFs w/o target flow]	-0.943 ± 0.032	-0.970 ± 0.072	-0.679 ± 0.061	-0.674 ± 0.091
KDE (Kim et al., 2018)	-0.942 ± 0.010	-0.948 ± 0.069	-0.700 ± 0.044	-0.708 ± 0.098
DKME (Muandet et al., 2021)	-0.940 ± 0.010	-0.952 ± 0.082	-0.665 ± 0.015	-0.670 ± 0.063
CNF+TS (Kennedy et al., 2023)	-1.000 ± 0.030	-1.056 ± 0.237	-0.683 ± 0.080	-0.668 ± 0.128
INFs w/o bias corr	-0.932 ± 0.013	-0.936 ± 0.112	-0.667 ± 0.028	-0.670 ± 0.067
INFs (main)	$\mathbf{-0.912 \pm 0.010}$	$\underline{-0.929 \pm 0.099}$	$\underline{-0.658 \pm 0.020}$	$\underline{-0.659 \pm 0.090}$

Higher = better (best in bold, second best underlined)

ACIC 2016 & 2018 datasets. ACIC 2016 & 2018 provide a collection of 77 and 24 semi-synthetic datasets, respectively, with various data-generating mechanisms (Dorie et al., 2019; Shimoni et al., 2018) (see details in Appendix H). We perform five random train/test splits (80%/20%) for each dataset, tune hyperparameters on the first split, and evaluate the average in- and out-sample log-probability on every split. Table 3 provides the performance comparison. Again, our INFs have a clear performance improvement over the baselines and other model variants. Compared to MDNs as the second-best method, our INFs scale much better in terms of runtime, especially for large sample sizes (see Appendix L).

Table 3. Results for ACIC 2016 and ACIC 2018. Reported: % of runs with the best performance.

	ACIC 2016 (77 datasets)		ACIC 2018 (24 datasets)	
	% best$_{\text{in}}$	% best$_{\text{out}}$	% best$_{\text{in}}$	% best$_{\text{out}}$
TARNet*	3.90%	6.23%	7.08%	7.50%
MDNs	28.96%	29.35%	21.25%	18.75%
CNF [≙ INFs w/o target flow]	14.42%	15.97%	14.17%	14.58%
KDE (Kim et al., 2018)	1.04%	1.04%	10.42%	9.58%
DKME (Muandet et al., 2021)	0.39%	0.78%	8.75%	10.83%
CNF+TS (Kennedy et al., 2023)	8.18%	8.96%	5.83%	5.42%
INFs w/o bias corr	5.45%	7.27%	4.58%	5.42%
INFs (main)	**37.66%**	**30.39%**	**27.92%**	**27.92%**

Higher = better (best in bold)

HC-MNIST dataset. Hidden confounding MNIST dataset (Jesson et al., 2021) is a semi-synthetic dataset constructed on top of the canonical image dataset of handwritten digits (MNIST) (LeCun, 1998). To satisfy the exchangeability assumption, we add a hidden confounder to the set of all covariates, i. e., 28x28 images ($d_X = 784 + 1$). Dataset details are in Appendix H. For our experiments, we use only the train subset of the original MNIST ($n = 42,000$). We use ten random train/test splits (80%/20%) and tune hyperparameters on the first split. Table 4 shows the results of the experiments. Note that the semi-parametric plug-in estimators suffer from scalability issues and are thus excluded. Further, our INFs outperform the variant without a bias correction and other available baselines.

Scalability. Experiments with ACIC 2018 and HC-MNIST datasets show the scalability of our INFs for datasets with large sample sizes ($n > 25,000$) and with high-dimensional covariates ($d_X > 100$). We provide a runtime comparison in Appendix L. For HC-MNIST, non- and semi-parametric methods become highly impractical due to memory and time constraints. For example, our INFs took ∼5 min per experiment, while KDE took ∼26 min and DKME ∼18 min. This is a major advantage of our fully-parametric IDE estimator (INFs) over semi-parametric plug-in estimators and other baselines.

Table 4. Results for HC-MNIST. Reported: mean ± sd over ten random train-test splits.

	$a=0$		$a=1$	
	log-prob$_{\text{in}}$	log-prob$_{\text{out}}$	log-prob$_{\text{in}}$	log-prob$_{\text{out}}$
KDE (Kim et al., 2018)	-1.354 ± 0.002	-1.354 ± 0.004	-1.380 ± 0.001	-1.382 ± 0.003
DKME (Muandet et al., 2021)	-1.471 ± 0.003	-1.467 ± 0.009	-1.395 ± 0.001	-1.398 ± 0.003
CNF+TS (Kennedy et al., 2023)	-1.368 ± 0.015	-1.370 ± 0.017	-1.331 ± 0.001	-1.335 ± 0.005
INFs w/o bias corr	-1.430 ± 0.181	-1.429 ± 0.181	-1.400 ± 0.171	-1.402 ± 0.170
INFs (main)	$\mathbf{-1.339 \pm 0.005}$	$\mathbf{-1.338 \pm 0.009}$	$\mathbf{-1.329 \pm 0.002}$	$\mathbf{-1.332 \pm 0.007}$

Higher = better (best in bold)

Case study. We performed a case study using data from California's tobacco control program to estimate its effect on tobacco sales. Previous evidence was primarily based on point estimates without information on the interventional density (Abadie et al., 2010). Our INFs suggest that the program would lead to a large reduction in tobacco sales (see Appendix M).

Discussion. Interestingly, both components of our INFs are important for the final performance (see our ablation studies). (i) The nuisance flow with the help of noise regularization performs consistent estimation of the nuisance parameters. (ii) The target flow uses estimated nuisance parameters to solve the optimization objective. In the overwhelming majority of experiments, a large part of the performance of our INFs are attributed to the second-stage estimation, i. e., the target flow. The target flow is also crucial for computational performance. While simple NFs have a similar estimation performance in terms of goodness-of-fit, only our INFs have constant inference time (e.g., during the evaluation phase regardless of the size of the training data). This is a major advantage of fully-parametric treatment effect estimators over semi-parametric plug-in estimators.

Regarding the choice of the normalizing flows, the neural spline flows are one of the possible choices of the universal density approximators.[10] We demonstrated that they outperform other baselines in the overwhelming majority of the experiments. We further advocate neural spline flows as they are both flexible and parsimonious.

Conclusion: For decision-making in personalized medicine, it is not only important to know what effect treatments have on patient health but also how likely it is that treatments achieve the desired outcome. To address this, we propose a novel method for estimating the density of potential outcomes. Specifically, we present our *Interventional Normalizing Flows*, which is the first, fully-parametric, deep learning method for this purpose.

[10] Universal and efficient high-dimensional density estimation is still an open problem in the deep learning community.

References

Abadie, A., Diamond, A., and Hainmueller, J. Synthetic control methods for comparative case studies: Estimating the effect of California's tobacco control program. *Journal of the American Statistical Association*, 105(490): 493–505, 2010.

Alaa, A. M. and van der Schaar, M. Bayesian inference of individualized treatment effects using multi-task Gaussian processes. In *Advances in Neural Information Processing Systems*, 2017.

Alaa, A. M. and van der Schaar, M. Bayesian nonparametric causal inference: Information rates and learning algorithms. *IEEE Journal of Selected Topics in Signal Processing*, 12(5):1031–1046, 2018.

Balgi, S., Pena, J. M., and Daoud, A. Personalized public policy analysis in social sciences using causal-graphical normalizing flows. In *Association for the Advancement of Artificial Intelligence*, 2022.

Bareinboim, E., Correa, J. D., Ibeling, D., and Icard, T. On Pearl's hierarchy and the foundations of causal inference. In *Probabilistic and Causal Inference: The Works of Judea Pearl*, pp. 507–556. Association for Computing Machinery, 2022.

Bellot, A. and van der Schaar, M. Policy analysis using synthetic controls in continuous-time. In *International Conference on Machine Learning*, 2021.

Bhattacharyya, A., Gayen, S., Kandasamy, S., Raval, V., and Variyam, V. N. Efficient interventional distribution learning in the PAC framework. In *International Conference on Artificial Intelligence and Statistics*, 2022.

Bica, I., Jordon, J., and van der Schaar, M. Estimating the effects of continuous-valued interventions using generative adversarial networks. In *Advances in Neural Information Processing Systems*, 2020.

Bica, I., Alaa, A. M., Lambert, C., and van der Schaar, M. From real-world patient data to individualized treatment effects using machine learning: current and future methods to address underlying challenges. *Clinical Pharmacology & Therapeutics*, 109:87–100, 2021.

Bickel, P. J., Klaassen, C. A., Ritov, Y., and Wellner, J. A. *Efficient and adaptive estimation for semiparametric models*, volume 4. Springer New York, NY, 1993.

Bishop, C. M. Mixture density networks. 1994.

Brouillard, P., Lachapelle, S., Lacoste, A., Lacoste-Julien, S., and Drouin, A. Differentiable causal discovery from interventional data. In *Advances in Neural Information Processing Systems*, 2020.

Chernozhukov, V., Chetverikov, D., Demirer, M., Duflo, E., Hansen, C., Newey, W., and Robins, J. Double/debiased machine learning for treatment and structural parameters. *The Econometrics Journal*, 21(1):C1–C68, 2018.

Curth, A. and van der Schaar, M. Nonparametric estimation of heterogeneous treatment effects: From theory to learning algorithms. In *International Conference on Artificial Intelligence and Statistics*, 2021.

Dinh, L., Krueger, D., and Bengio, Y. NICE: Non-linear independent components estimation. *arXiv preprint arXiv:1410.8516*, 2014.

Dinh, L., Sohl-Dickstein, J., and Bengio, S. Density estimation using real NVP. In *International Conference on Learning Representations*, 2017.

Dolatabadi, H. M., Erfani, S., and Leckie, C. Invertible generative modeling using linear rational splines. In *International Conference on Artificial Intelligence and Statistics*, 2020.

Dorie, V., Hill, J., Shalit, U., Scott, M., and Cervone, D. Automated versus do-it-yourself methods for causal inference: Lessons learned from a data analysis competition. *Statistical Science*, 34(1):43–68, 2019.

Durkan, C., Bekasov, A., Murray, I., and Papamakarios, G. Neural spline flows. In *Advances in Neural Information Processing Systems*, 2019.

Efromovich, S. Orthogonal series density estimation. *Wiley Interdisciplinary Reviews: Computational Statistics*, 2(4): 467–476, 2010.

Garreau, D., Jitkrittum, W., and Kanagawa, M. Large sample analysis of the median heuristic. *arXiv preprint arXiv:1707.07269*, 2017.

Gellerstedt, K. and Sjölin, J. Analysis of scattered higher dimensional data using generalized fourier interpolation. *arXiv preprint arXiv:2202.13801*, 2022.

Gische, C. and Voelkle, M. C. Beyond the mean: A flexible framework for studying causal effects using linear models. *Psychometrika*, 87:868–901, 2021.

Grünewälder, S., Lever, G., Gretton, A., Baldassarre, L., Patterson, S., and Pontil, M. Conditional mean embeddings as regressors. In *International Conference on Machine Learning*, 2012.

Ha, D., Dai, A. M., and Le, Q. V. HyperNetworks. In *International Conference on Learning Representations*, 2017.

Hassanpour, N. and Greiner, R. Learning disentangled representations for counterfactual regression. In *International Conference on Learning Representations*, 2019.

Hatt, T. and Feuerriegel, S. Estimating average treatment effects via orthogonal regularization. In *International Conference on Information and Knowledge Management*, 2021.

Hatt, T., Berrevoets, J., Curth, A., Feuerriegel, S., and van der Schaar, M. Combining observational and randomized data for estimating heterogeneous treatment effects. *arXiv preprint arXiv:2202.12891*, 2022.

Hill, J. L. Bayesian nonparametric modeling for causal inference. *Journal of Computational and Graphical Statistics*, 20(1):217–240, 2011.

Hirst, J. A., Farmer, A. J., Ali, R., Roberts, N. W., and Stevens, R. J. Quantifying the effect of metformin treatment and dose on glycemic control. *Diabetes Care*, 35 (2):446–454, 2012.

Huang, C.-W., Krueger, D., Lacoste, A., and Courville, A. Neural autoregressive flows. In *International Conference on Machine Learning*, 2018.

Hünermund, P., Kaminski, J. C., and Schmitt, C. Causal machine learning and business decision making. In *Academy of Management Proceedings*, 2021.

Ilse, M., Forré, P., Welling, M., and Mooij, J. M. Combining interventional and observational data using causal reductions. *arXiv preprint arXiv:2103.04786*, 2021.

Jesson, A., Mindermann, S., Shalit, U., and Gal, Y. Identifying causal-effect inference failure with uncertainty-aware models. In *Advances in Neural Information Processing Systems*, 2020.

Jesson, A., Mindermann, S., Gal, Y., and Shalit, U. Quantifying ignorance in individual-level causal-effect estimates under hidden confounding. In *International Conference on Machine Learning*, 2021.

Jesson, A., Douglas, A. R., Manshausen, P., Solal, M., Meinshausen, N., Stier, P., Gal, Y., and Shalit, U. Scalable sensitivity and uncertainty analyses for causal-effect estimates of continuous-valued interventions. In *Advances in Neural Information Processing Systems*, 2022.

Johansson, F., Shalit, U., and Sontag, D. Learning representations for counterfactual inference. In *International Conference on Machine Learning*, 2016.

Kennedy, E. H. Optimal doubly robust estimation of heterogeneous causal effects. *arXiv preprint arXiv:2004.14497*, 2020.

Kennedy, E. H. Semiparametric doubly robust targeted double machine learning: A review. *arXiv preprint arXiv:2203.06469*, 2022.

Kennedy, E. H., Balakrishnan, S., and Wasserman, L. Semiparametric counterfactual density estimation. *Biometrika*, 2023.

Khemakhem, I., Monti, R., Leech, R., and Hyvarinen, A. Causal autoregressive flows. In *International Conference on Artificial Intelligence and Statistics*, 2021.

Kim, K., Kim, J., and Kennedy, E. H. Causal effects based on distributional distances. *arXiv preprint arXiv:1806.02935*, 2018.

Kingma, D. P. and Ba, J. Adam: A method for stochastic optimization. In *International Conference on Learning Representations*, 2015.

Kingma, D. P. and Welling, M. Auto-encoding variational Bayes. *arXiv preprint arXiv:1312.6114*, 2013.

Künzel, S. R., Sekhon, J. S., Bickel, P. J., and Yu, B. Metalearners for estimating heterogeneous treatment effects using machine learning. *Proceedings of the National Academy of Sciences*, 116(10):4156–4165, 2019.

Kuzmanovic, M., Hatt, T., and Feuerriegel, S. Estimating conditional average treatment effects with missing treatment information. In *International Conference on Artificial Intelligence and Statistics*, 2023.

LeCun, Y. The MNIST database of handwritten digits. *http://yann.lecun.com/exdb/mnist/*, 1998.

MacDorman, M. and Atkinson, J. Infant mortality statistics from the linked birth/infant death data set–1995 period data. *Monthly Vital Statistics Report*, 46(6 Suppl 2):1–22, 1998.

Muandet, K., Kanagawa, M., Saengkyongam, S., and Marukatat, S. Counterfactual mean embeddings. *Journal of Machine Learning Research*, 22:1–71, 2021.

Müller, J., Schmier, R., Ardizzone, L., Rother, C., and Köthe, U. Learning robust models using the principle of independent causal mechanisms. In *DAGM German Conference on Pattern Recognition*, 2021.

Nie, L., Ye, M., Liu, Q., and Nicolae, D. VCNet and functional targeted regularization for learning causal effects of continuous treatments. In *International Conference on Learning Representations*, 2021.

Niswander, K. R. The collaborative perinatal study of the National Institute of Neurological Diseases and Stroke. *The Woman and Their Pregnancies*, 1972.

Pearl, J. *Causality*. Cambridge university press, 2009.

Polyak, B. T. and Juditsky, A. B. Acceleration of stochastic approximation by averaging. *SIAM Journal on Control and Optimization*, 30(4):838–855, 1992.

Ranganath, R., Tang, L., Charlin, L., and Blei, D. Deep exponential families. In *International Conference on Artificial Intelligence and Statistics*, 2015.

Rezende, D. and Mohamed, S. Variational inference with normalizing flows. In *International Conference on Machine Learning*, 2015.

Robins, J. M. Robust estimation in sequentially ignorable missing data and causal inference models. In *Proceedings of the American Statistical Association*, 2000.

Robins, J. M. and Rotnitzky, A. Comment on the Bickel and Kwon article, "Inference for semiparametric models: Some questions and an answer". *Statistica Sinica*, 11(4): 920–936, 2001.

Rothfuss, J., Ferreira, F., Boehm, S., Walther, S., Ulrich, M., Asfour, T., and Krause, A. Noise regularization for conditional density estimation. *arXiv preprint arXiv:1907.08982*, 2019.

Rubin, D. B. Estimating causal effects of treatments in randomized and nonrandomized studies. *Journal of Educational Psychology*, 66(5):688, 1974.

Schwab, P., Linhardt, L., Bauer, S., Buhmann, J. M., and Karlen, W. Learning counterfactual representations for estimating individual dose-response curves. In *AAAI Conference on Artificial Intelligence*, 2020.

Schweisthal, J., Frauen, D., Melnychuk, V., and Feuerriegel, S. Reliable off-policy learning for dosage combinations. *arXiv preprint arXiv:2305.19742*, 2023.

Shalit, U., Johansson, F. D., and Sontag, D. Estimating individual treatment effect: generalization bounds and algorithms. In *International Conference on Machine Learning*, 2017.

Shi, C., Blei, D., and Veitch, V. Adapting neural networks for the estimation of treatment effects. In *Advances in Neural Information Processing Systems*, 2019.

Shimoni, Y., Yanover, C., Karavani, E., and Goldschmnidt, Y. Benchmarking framework for performance-evaluation of causal inference analysis. *arXiv preprint arXiv:1802.05046*, 2018.

Shin, J.-I. Second-line glucose-lowering therapy in type 2 diabetes mellitus. *Current Diabetes Reports*, 19:1–9, 2019.

Shpitser, I. and Pearl, J. What counterfactuals can be tested. In *Conference on Uncertainty in Artificial Intelligence*, 2007.

Spiegelhalter, D. Risk and uncertainty communication. *Annual Review of Statistics and Its Application*, 4(1):31–60, 2017.

Tabak, E. G. and Vanden-Eijnden, E. Density estimation by dual ascent of the log-likelihood. *Communications in Mathematical Sciences*, 8(1):217–233, 2010.

Titterington, D. M., Afm, S., Smith, A. F., Makov, U., et al. *Statistical analysis of finite mixture distributions*, volume 198. John Wiley & Sons Incorporated, 1985.

Trippe, B. L. and Turner, R. E. Conditional density estimation with Bayesian normalising flows. *arXiv preprint arXiv:1802.04908*, 2018.

van der Bles, A. M., van der Linden, S., Freeman, A. L., Mitchell, J., Galvao, A. B., Zaval, L., and Spiegelhalter, D. J. Communicating uncertainty about facts, numbers and science. *Royal Society Open Science*, 6(5):181870, 2019.

van der Laan, M. J. and Robins, J. M. *Unified methods for censored longitudinal data and causality*, volume 5. Springer New York, NY, 2003.

van der Laan, M. J. and Rubin, D. Targeted maximum likelihood learning. *The International Journal of Biostatistics*, 2(1):Article 11, 2006.

van der Laan, M. J., Rose, S., et al. *Targeted learning: Causal inference for observational and experimental data*, volume 10. Springer, 2011.

Vowels, M. J., Akbari, S., Camgoz, N. C., and Bowden, R. A free lunch with influence functions? Improving neural network estimates with concepts from semiparametric statistics. *arXiv preprint arXiv:2202.09096*, 2022.

Wager, S. and Athey, S. Estimation and inference of heterogeneous treatment effects using random forests. *Journal of the American Statistical Association*, 113(523):1228–1242, 2018.

Wang, R., Chaudhari, P., and Davatzikos, C. Harmonization with flow-based causal inference. In *International Conference on Medical Image Computing and Computer-Assisted Intervention*, 2021.

Wehenkel, A. and Louppe, G. Graphical normalizing flows. In *International Conference on Artificial Intelligence and Statistics*, 2021.

Yang, J., Eckles, D., Dhillon, P., and Aral, S. Targeting for long-term outcomes. *arXiv preprint arXiv:2010.15835*, 2020.

Zhang, Y., Bellot, A., and van der Schaar, M. Learning overlapping representations for the estimation of individualized treatment effects. In *International Conference on Artificial Intelligence and Statistics*, 2020.

A. Related work: Normalizing flows for causal inference

NFs have been used in the wider area of causal inference, yet in vastly *different* tasks than ours. Examples include, e. g., robust prediction by employing causal mechanisms (Müller et al., 2021); combining interventional and observational datasets (Ilse et al., 2021); and causal discovery (Brouillard et al., 2020). Further, several works aim to model Bayesian networks or structural causal models (SCMs) with known or unknown causal diagrams. For example, NFs were used as a probabilistic model for Bayesian networks aimed at causal discovery, as well as downstream interventional and counterfactual inference (Khemakhem et al., 2021; Wang et al., 2021; Wehenkel & Louppe, 2021). Balgi et al. (2022) build upon a temporal SCM with exogenous noise, where NFs are used for interventional and counterfactual queries. Importantly, all the aforementioned methods assume continuous variables in SCMs and *independence of exogenous noise*.[11] Hence, these methods are **not** applicable in our case, which considers semi-Markovian SCMs and which is thus a different inference task.[12] In sum, NFs have not yet been adapted to IDE, which is our novelty.

[11]This is commonly known as a causal Markov condition.

[12]This is stated in our identifiability assumptions: there is no limitation on the exogenous noise independence between outcome and covariates. Hence, our setting is more general.

B. Background materials

B.1. Normalizing flows

Normalizing flows (NFs) (Tabak & Vanden-Eijnden, 2010; Rezende & Mohamed, 2015) are flexible probabilistic models with a tractable density. A normalizing flow describes the change of the density of a continuous random variable after applying a sequence of invertible transformations. Given a random variable Z with some known density $\mathbb{P}(Z = \cdot)$, e. g., normal or uniform, we define a transformed variable

$$X = t(Z) \quad Z \sim \mathbb{P}(Z), \tag{16}$$

where $t(\cdot) : \mathcal{Z} \to \mathcal{X}$ denotes an invertible forward transformation with inverse $t^{-1}(\cdot) : \mathcal{X} \to \mathcal{Z}$. Importantly, the transformation is defined between spaces of the same dimensionality $d_Z = d_X$. To find a distribution of X, we can apply the multivariate *change of variables formula*

$$\mathbb{P}(X = x) = \mathbb{P}(Z = z) \left| \det \frac{\mathrm{d}Z}{\mathrm{d}X} \right| = \mathbb{P}(Z = t^{-1}(x)) \left| \det \frac{\mathrm{d}t^{-1}}{\mathrm{d}X}(x) \right|, \tag{17}$$

where $\det \frac{\mathrm{d}t^{-1}}{\mathrm{d}X}(x)$ is the Jacobian determinant of the inverse transformation $t^{-1}(\cdot)$. Then, using the *inverse function theorem*, we obtain

$$\frac{\mathrm{d}t^{-1}}{\mathrm{d}X} = \left(\frac{\mathrm{d}t}{\mathrm{d}Z} \right)^{-1}, \tag{18}$$

so that the Jacobian of the inverse transformation can be substituted with the inverse Jacobian of forward transformation. Using the properties of the determinant, Eq. (17) can be simplified to

$$\mathbb{P}(X = x) = \mathbb{P}(Z = t^{-1}(x)) \left| \det \frac{\mathrm{d}t}{\mathrm{d}Z}\big(t^{-1}(x)\big) \right|^{-1}. \tag{19}$$

The name *normalizing* comes from the fact that any regular continuous distribution X can be transformed to a normal Z with a specific $t^{-1}(\cdot)$.

We can construct arbitrarily complex densities by applying a composition of K transformations $t_1, t_2, \ldots, t_K$:

$$X = Z_K = t_K(Z_{K-1}) = t_K(t_{K-1}(Z_{K-2})) = \ldots = t_K \circ \ldots \circ t_1(Z_0), \tag{20}$$

where Z_0 is called a base distribution. One calls this chain of transformations a *flow*. Finally, the density of X can be recursively found as

$$\mathbb{P}(Z_K = z_K) = \mathbb{P}(Z_{K-1} = z_{K-1}) \left| \det \frac{\mathrm{d}t_K}{\mathrm{d}Z_{K-1}}(z_{K-1}) \right|^{-1} = \mathbb{P}(Z_0 = z_0) \prod_{k=1}^{K} \left| \det \frac{\mathrm{d}t_k}{\mathrm{d}Z_{k-1}}(z_{k-1}) \right|^{-1}, \tag{21}$$

where $z_0, z_1, \ldots, z_K$ are found via Eq. (20). Consequently, we now can directly evaluate the log-likelihood of an observation $X_i = Z_{Ki}$ and, with a proper parametrization of transformations, back-propagate through it. Examples of simple transformations include affine, planar, and radial (Rezende & Mohamed, 2015).

B.2. Causal model and identification

In this section, we provide a brief background on the underlying causal model in this paper, using both the potential outcomes and the structural causal model framework. These frameworks are equivalent in the sense that they both allow for identification of the interventional density and yield the same statistical estimand.

Potential outcomes framework. The observed variables in our model are covariates $X \in \mathcal{X} \subseteq \mathbb{R}^{d_X}$, a treatment $A \in \{0, 1\}$, and a d_Y-dimensional continuous outcome $Y \in \mathcal{Y} \subseteq \mathbb{R}^{d_Y}$. In the main paper, we used the potential outcomes framework (Rubin, 1974) to define the causal estimates. In particular, we defined $Y[a]$ as the potential outcome after intervening on treatment by setting it to a. By imposing Assumptions (1)–(3) in Section 3, this allows us to define the interventional density (our causal estimand) via

$$\mathbb{P}(Y[a] = y) = \int_{x \in \mathcal{X}} \mathbb{P}(Y = y \mid X = x, A = a)\, \mathbb{P}(X = x)\, \mathrm{d}x = \mathop{\mathbb{E}}_{X \sim \mathbb{P}(X)} \big(\mathbb{P}(Y = y \mid X, A = a) \big). \tag{22}$$

SCM framework. Equivalently to the potential outcomes framework, we can also define the interventional density within the structural causal model (SCM) framework (Pearl, 2009; Bareinboim et al., 2022). More precisely, we can define a (semi-Markovian) SCM by introducing independent exogenous latent variables $U_A \sim \mathbb{P}(U_A)$ and $U_{XY} \sim \mathbb{P}(U_{XY})$; and the functional assignments $X := f_X(U_{XY})$, $A := f_A(X, U_A)$, and $Y := f_Y(X, U_{XY})$. Here, X, A and Y are observed endogenous variables, satisfying Assumptions (1)–(3). We show a corresponding causal diagram $\mathcal{G}$ in Fig. 4.

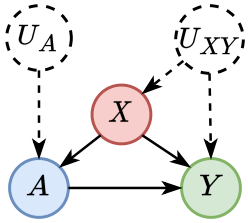

Figure 4. Causal diagram $\mathcal{G}$ corresponding to the potential outcome framework assumptions.

Interventions vs. counterfactuals. We follow Pearl's hierarchy on causal inference (Bareinboim et al., 2022) and distinguish the *interventional* and the *counterfactual* distribution. In SCM language, we can use Pearl's do-notation $do(A = a)$ to denote an intervention on the treatment A. This corresponds to setting $A = a$ in a diagram $\mathcal{G}$ where all arrows leading to A are removed.

We can then define the potential outcome $Y[a]$ via its interventional density

$$\mathbb{P}(Y[a] = y) = \mathbb{P}(Y = y \mid do(A = a)) \tag{23}$$

and obtain the identification result from Eq. (22).

In contrast, the *counterfactual* density aims to answer *individualized* questions "what would have happened if we had used a different treatment a for the population, which already received treatment a'":

$$\mathbb{P}(Y[a] = y \mid A = a') \tag{24}$$

where $a' \neq a$. If the treatment is binary, the counterfactual density can be expressed in terms of interventional and observational densities:[13]

$$\mathbb{P}(Y[a] = y \mid A = a') = \frac{1}{\mathbb{P}(A = a')} \Big(\mathbb{P}(Y[a] = y) - \mathbb{P}(Y = y \mid A = a)\mathbb{P}(A = a) \Big). \tag{25}$$

This is the distributional equivalent to the average treatment effect of the treated (ATT). However, most of the treatment effect estimation literature focuses on *interventional* causal estimands (such as the ATE). Our paper is therefore in line with previous work. We acknowledge that other papers oftentimes call the interventional distribution counterfactual distributions for simplicity.

Comparison to other identification strategies. For the identification of the interventional density, we mainly rely on the three main assumptions of positivity, consistency, and exchangeability (or, equivalently, on the back-door adjustment from Eq. (22)). This is a common setup in treatment effect estimation (van der Laan & Rubin, 2006; Shalit et al., 2017; Wager & Athey, 2018). More complex adjustment rules (e.g., front-door adjustment, adjustment for napkin graph) have the following limitations: (1) they require more unusual, complex assumptions which are often violated in practice; and (2) they require a complex efficient estimation theory Vowels et al. (2022). Nevertheless, this could be an interesting direction for future research.

B.3. Efficiency theory and influence functions

In this section, we give a brief background on semi-parametric efficiency theory and influence functions. Our background builds upon Kennedy et al. (2023), and we thus refer to it for mathematical details and further explanations.

[13] In the case of categorical treatment, additional identification assumptions are required, e. g., the exact knowledge of SCM (Shpitser & Pearl, 2007).

Let us consider a semi-parametric statistical model $\{\mathbb{P} \in \mathcal{P}\}$, where $\mathcal{P}$ is a family of probability measures. We are interested in estimating a functional $\psi \colon \mathcal{P} \to \mathbb{R}$. If ψ is sufficiently smooth, it admits the so-called *von Mises* or *distributional Taylor expansion*

$$\psi(\bar{\mathbb{P}}) - \psi(\mathbb{P}) = \int \phi(t, \bar{\mathbb{P}}) \, \mathrm{d}(\bar{\mathbb{P}} - \mathbb{P})(t) + R_2(\bar{\mathbb{P}}, \mathbb{P}), \tag{26}$$

where $R_2(\bar{\mathbb{P}}, \mathbb{P})$ is a *second-order remainder term* and $\phi(t, \mathbb{P})$ is the so-called *efficient influence function* of ψ, satisfying $\int \phi(t, \mathbb{P}) d\mathbb{P}(t) = 0$ and $\int \phi(t, \mathbb{P})^2 d\mathbb{P}(t) < \infty$.

The efficient influence function $\phi(\cdot, \cdot)$ plays an important role in the theory of efficient semi-parametric estimation. Under certain assumptions, it can be shown that, for any sequence of estimators $\hat{\psi}_n$, it holds that

$$\inf_{\delta > 0} \liminf_{n \to \infty} \sup_{\mathrm{TV}(\mathbb{P}, \mathbb{Q}) < \delta} n \, \mathbb{E}_{\mathbb{Q}} \left[(\hat{\psi}_n - \psi(\mathbb{Q}))^2 \right] \geq \mathrm{var}\left(\phi(T, \mathbb{P})\right), \tag{27}$$

where TV denotes total variation. Hence, ϕ characterizes the best possible variance an estimator can achieve (in a local min-max sense).

Let now $\hat{\mathbb{P}}$ be an estimator of $\mathbb{P}$ and $\psi(\hat{\mathbb{P}})$ the so-called *plug-in estimator* of $\psi(P)$. The von Mises expansion from Eq. (26) implies that $\psi(\hat{\mathbb{P}})$ yields a first-order *plug-in bias* because

$$\psi(\hat{\mathbb{P}}) - \psi(\mathbb{P}) = -\int \phi(t, \hat{\mathbb{P}}) \, \mathrm{d}\mathbb{P}(t) + R_2(\hat{\mathbb{P}}, \mathbb{P}) \tag{28}$$

due to that $\int \phi(t, \hat{\mathbb{P}}) \, \mathrm{d}\hat{\mathbb{P}}(t) = 0$. A simple way to correct for the plug-in bias is to estimate the bias term from the right-hand side of Eq. (28) and add it to the plug-in estimator via

$$\hat{\psi}^{\text{A-IPTW}} = \psi(\hat{\mathbb{P}}) + \mathbb{P}_n(\phi(T, \hat{\mathbb{P}})). \tag{29}$$

Under certain assumptions, it can be shown that the bias-corrected estimator $\hat{\psi}^{\text{A-IPTW}}$ is asymptotically normal with mean zero and variance $\mathrm{var}\left(\phi(T, \mathbb{P})\right)$. Hence, by Eq. (27), $\hat{\psi}^{\text{A-IPTW}}$ is (asymptotically) *efficient* in the sense that it is consistent with the best possible variance.

Application to interventional density estimation: We now return to the specific statistical model in our paper, i.e., we aim at interventional density estimation. In other words, the estimand $\psi(\mathbb{P})$ we are interested in is the function

$$\mathbb{P}(Y[a] = \cdot) = \mathop{\mathbb{E}}_{X \sim \mathbb{P}(X)} \big(\mathbb{P}(Y = \cdot \mid X, A = a) \big). \tag{30}$$

Given an initial estimator $\hat{\mathbb{P}}(Y = \cdot \mid X, A = a)$ and the marginal empirical probability measure $\mathbb{P}_n\{\cdot\}$, the plug-in estimator becomes

$$\hat{\mathbb{P}}^{\text{PI}}(Y[a] = \cdot) = \mathbb{P}_n\{\hat{\mathbb{P}}(Y = \cdot \mid X, A = a)\}. \tag{31}$$

As described above, this estimator suffers from plug-in bias and is not efficient. However, a one-step bias correction for our setting is <u>not</u> as simple due to the fact that the interventional density is a functional target estimand and, hence, infinite-dimensional. As a remedy, Kennedy et al. (2023) proposes an elegant solution by introducing the finite-dimensional projection parameter

$$\hat{\beta}_a = \arg\min_{\beta_a} \mathrm{KL} \left(\mathbb{P}(Y[a]) \, \middle\| \, g(\cdot; \beta_a) \right), \tag{32}$$

which is equivalent to solving the moment condition

$$m(\beta_a) = \mathop{\mathbb{E}}_{X \sim \mathbb{P}(X)} \Big(\mathbb{E}\big(T(Y; \beta_a) \mid X, A = a \big) \Big) \stackrel{!}{=} 0, \tag{33}$$

where $T = T(Y; \beta_a) = -\nabla_{\beta_a} \log g(Y; \beta_a)$. The advantage of this approach is that the moment $m(\beta_a)$ is a finite-dimensional quantity, which means efficiency theory can be applied. The plug-in estimator for the moment is

$$\hat{m}^{\text{PI}}(\beta_a) = \mathop{\mathbb{E}}_{\hat{Y}^a \sim \mathbb{P}_n\{\hat{\mathbb{P}}(Y \mid X, A = a)\}} T(\hat{Y}^a; \beta_a). \tag{34}$$

Kennedy et al. (2023) also derived the efficient influence function for the moment:

$$\phi_a(T;\mathbb{P}) = \frac{\mathbb{1}(A=a)}{\pi_a(X)}\Big(T - \mathbb{E}(T \mid X, A=a)\Big) + \mathbb{E}(T \mid X, A=a) - \underset{X\sim\mathbb{P}(X)}{\mathbb{E}}(\mathbb{E}(T \mid X, A=a)). \tag{35}$$

Hence, a bias-corrected estimator for the projection parameter can be obtained by solving

$$\hat{m}^{\text{A-IPTW}}(\beta_a) = \hat{m}^{\text{PI}}(\beta_a) + \mathbb{P}_n\big\{\phi_a(T(Y;\beta_a);\hat{\mathbb{P}})\big\} \stackrel{!}{=} 0. \tag{36}$$

Estimating the projection parameter via Eq. (36) requires solving a (potentially high-dimension) system of non-linear equations, which is often infeasible in practice. Hence, as a remedy, we propose in this paper to reformulate Eq. (36) as an optimization problem which can be incorporated directly into the loss of a neural network (see Appendix C).

C. Bias-corrected moment condition as an optimization task

We aim to transform the bias-corrected moment condition into an optimization objective:

$$\hat{m}^{\text{A-IPTW}}(\beta_a) = \hat{m}^{\text{PI}}(\beta_a) + \mathbb{P}_n\big\{\phi_a(T(Y;\beta_a);\hat{\mathbb{P}})\big\} \stackrel{!}{=} 0. \tag{37}$$

We first note that the plug-in estimator of moment condition $\hat{m}^{\text{PI}}(\beta_a)$ can be rewritten as

$$\hat{m}^{\text{PI}}(\beta_a) = \mathop{\mathbb{E}}_{\hat{Y}^a \sim \mathbb{P}_n\{\hat{\mathbb{P}}(Y|X,A=a)\}} T(\hat{Y}^a;\beta_a) = \int_{\mathcal{Y}} T(y;\beta_a)\, \mathbb{P}_n\{\hat{\mathbb{P}}(Y=y \mid X, A=a)\}\,\mathrm{d}y \tag{38}$$

$$= \mathbb{P}_n\Big\{\int_{\mathcal{Y}} T(y;\beta_a)\,\hat{\mathbb{P}}(Y=y \mid X, A=a)\,\mathrm{d}y\Big\} = \mathbb{P}_n\Big\{\hat{\mathbb{E}}\big(T(Y;\beta_a) \mid X, A=a\big)\Big\}, \tag{39}$$

where the last equality follows from the definition of the conditional expectation. Notably, we see that the moment condition could be equivalently solved with either the conditional distribution, $\mathbb{P}(Y \mid X, A=a)$, or with the functional regression, $\mathbb{E}\big(T(Y;\beta_a) \mid X, A=a\big)$.

Let us unroll the bias correction term of Eq. (7):

$$\mathbb{P}_n\{\phi_a(T;\hat{\mathbb{P}})\} = \mathbb{P}_n\Big\{\frac{\mathbb{1}(A=a)}{\hat{\pi}_a(X)}\Big(T - \hat{\mathbb{E}}(T \mid X, A=a)\Big) + \hat{\mathbb{E}}(T \mid X, A=a) - \mathbb{P}_n\big\{\hat{\mathbb{E}}(T \mid X, A=a))\big\}\Big\} \tag{40}$$

$$= \mathbb{P}_n\Big\{\frac{\mathbb{1}(A=a)}{\hat{\pi}_a(X)}\Big(T - \hat{\mathbb{E}}(T \mid X, A=a)\Big) + \hat{\mathbb{E}}(T \mid X, A=a)\Big\} - \mathbb{P}_n\big\{\hat{\mathbb{E}}(T \mid X, A=a))\big\}, \tag{41}$$

where nuisance parameters are marked with red color. Here, the last term is, in fact, the plug-in estimator of the moment condition, i. e., $-\hat{m}^{\text{PI}}(\beta_a)$. Therefore, we can simplify the one-step bias corrected moment condition via

$$\hat{m}^{\text{A-IPTW}}(\beta_a) = \mathbb{P}_n\Big\{\frac{\mathbb{1}(A=a)}{\hat{\pi}_a(X)}\Big(T - \hat{\mathbb{E}}(T \mid X, A=a)\Big) + \hat{\mathbb{E}}(T \mid X, A=a)\Big\} \tag{42}$$

$$= \mathop{\mathbb{E}}_{\hat{Y}^a \sim \mathbb{P}_n\{\hat{\mathbb{P}}(Y|X,A=a)\}} T(\hat{Y}^a;\beta_a) + \mathbb{P}_n\Big\{\frac{\mathbb{1}(A=a)}{\hat{\pi}_a(X)}\Big(T(Y;\beta_a) - \mathop{\mathbb{E}}_{Y \sim \hat{\mathbb{P}}(Y|X,A=a)} T(Y;\beta_a)\Big)\Big\}, \tag{43}$$

where we use the conditional density estimator but not an estimator for the functional regression. This allows us to transform the A-IPTW moment condition into an optimization objective (Eq. (13)) by taking antiderivative with respect to β_a.

D. Two-step training procedure

Algorithm. Our INFs are trained with a two-step procedure. The procedure is shown in Algorithm 1. Recall that we use noise regularization as the main regularization technique for the nuisance flow, and exponential moving average (EMA) for the target flow to stabilize training. A-IPTW estimation is also known to become unstable in a finite sample setting (Shi et al., 2019), so that inverse values of propensity score become too large. Thus, we manually discard observations with too small propensity score ($\hat{\pi}_a(X) < 0.05$) from bias correction.

Algorithm 1 Training procedure of INFs

Input: number of iterations $n_{\text{iter,N}}, n_{\text{iter,T}}$; minibatch sizes $b_{\text{N}}, b_{\text{T}}$; learning rates $\eta_{\text{N}}, \eta_{\text{T}}$; intensities of the noise regularization σ_x^2, σ_y^2; EMA smoothing γ; grid size K.

Init: parameters of the nuisance flow: $\text{FC}_1^{(0)}, \text{FC}_2^{(0)}$ {Fitting the nuisance flow}

for $i = 0$ **to** $n_{\text{iter,N}}$ **do**

  $\mathcal{B} = \{X, A, Y\} \leftarrow$ minibatch of size b_{N}

  $R, \hat{\pi}_a(X) \leftarrow \text{FC}_1^{(i)}(X)$

  $\xi_x \sim N(0, \sigma_x^2); \quad \xi_y \sim N(0, \sigma_y^2); \quad \tilde{R} \leftarrow R + \xi_x; \quad \tilde{Y} \leftarrow Y + \xi_y$ {Noise regularization}

  $\theta(X, A) \leftarrow \text{FC}_2^{(i)}(A, \tilde{R})$

  $\hat{\mathbb{P}}(Y \mid X, A) \leftarrow$ normalizing flow with parameters $\theta(X, A)$

  $\mathcal{L}_{\text{NLL}} \leftarrow -\log \hat{\mathbb{P}}(Y = \tilde{Y} \mid X, A)$

  $\mathcal{L}_{\pi} \leftarrow \text{BCE}(\hat{\pi}_A(X), A)$

  $\mathcal{L}_{\text{N}}(\hat{\mathbb{P}}, \hat{\pi}_a) \leftarrow \mathbb{P}_{b_{\text{N}}}^{\mathcal{B}}\{\mathcal{L}_{\text{NLL}} + \alpha \mathcal{L}_{\pi}\}$

  $\text{FC}_1^{(i+1)}, \text{FC}_2^{(i+1)} \leftarrow$ optimization step wrt. $\mathcal{L}_{\text{N}}(\hat{\mathbb{P}}, \hat{\pi}_a)$ with learning rate η_{N}

end for

Output: nuisance parameters: $\hat{\mathbb{P}}(Y \mid X, A), \hat{\pi}_a(X)$

Init: parameters of the target flows: $\beta_a^{(0)}, \beta_{a,\text{EMA}}^{(0)} \leftarrow \beta_a^{(0)}$ {Fitting the target flows}

for $i = 0$ **to** $n_{\text{iter,T}}$ **do**

  $\mathcal{B} = \{X, A, Y\} \leftarrow$ minibatch of size b_{T}

  for $a \in \{0, 1\}$ **do**

    $\mathcal{L}_{\text{CE}}(\beta_a^{(i)}) \leftarrow -h \sum_{j=1}^{K} \log g(y_j; \beta_a^{(i)}) \mathbb{P}_{b_{\text{T}}}^{\mathcal{B}}\{\hat{\mathbb{P}}(Y = y_j \mid X, A = a)\}$

    $\mathcal{L}_{\text{CCE}}(X; \beta_a^{(i)}) \leftarrow -h \sum_{j=1}^{K} \log g(y_j; \beta_a^{(i)}) \hat{\mathbb{P}}(Y = y_j \mid X, A = a)$

    bias correction$(\beta_a^{(i)}) \leftarrow \mathbb{P}_{b_{\text{T}}}^{\mathcal{B}}\left\{ \frac{\mathbb{1}(A=a \& \hat{\pi}_a(X) \geq 0.05)}{\hat{\pi}_a(X)} \Big(-\log g(Y; \beta_a^{(i)}) - \mathcal{L}_{\text{CCE}}(X; \beta_a^{(i)}) \Big) \right\}$

    $\mathcal{L}_{\text{T}}(\beta_a^{(i)}) \leftarrow \mathcal{L}_{\text{CE}}(\beta_a^{(i)})$+bias correction$(\beta_a^{(i)})$

    $\beta_a^{(i+1)} \leftarrow$ optimization step wrt. $\mathcal{L}_{\text{T}}(\beta_a^{(i)})$ with learning rate η_{T}

    $\beta_{a,\text{EMA}}^{(i+1)} \leftarrow \gamma \beta_{a,\text{EMA}}^{(i)} + (1 - \gamma) \beta_a^{(i+1)}$ {EMA update}

  end for

end for

Output: $\hat{\beta}_a^{\text{A-IPTW}} \leftarrow \beta_{a,\text{EMA}}^{(n_{\text{iter,T}})}$

Differences to standard two-step meta-learners. There are two key differences between our nuisance-target model and standard two-step meta-learners (e. g., Curth & van der Schaar, 2021): (1) We aim to estimate the density of the non-individualized potential outcomes after an intervention. Standard two-step meta-learners are designed to estimate individualized causal estimands, e. g., CATE using the doubly robust (DR) learner. However, it is *not* standard in the literature to train a second model for non-individualized causal estimands (e. g., ATE). Here, standard practice is to simply average estimated nuisance parameters, thereby only leveraging the first step (e. g., A-IPTW estimator). In contrast, our approach is to train a second model for estimating the target causal estimand, i. e., our target flow. (2) Meta-learners for CATE estimation (e. g., DR learner) infer adjusted pseudo-outcomes once and use them to fit a second-step model. Our target flow (second-step model) needs access to the nuisance flow to estimate the A-IPTW adjusted objective from Eq. (15). This is different from the standard second-step CATE estimation, as we do not deal with a single pseudo-outcome, but with a full continuum of pseudo-outcomes, i. e., conditional distribution. Therefore, the second-step model requires extra computational heuristics, e. g., a feasible way to approximate the cross-entropy and smoothing of the training with

minibatches (see Appendix E). To the best of our knowledge, this kind of learning was not implemented or evaluated before in the context of two-step causal inference.

E. INFs implementation details

Implementation. We implemented our INFs using PyTorch and Pyro. For both the nuisance and target flow, we employ neural spline flows (Durkan et al., 2019) with standard normal, $N(0, 1)$, as a base distribution. Neural spline flows construct an invertible transformation of the base distribution with the help of monotonic rational-quadratic splines. They are characterized by two main hyperparameters: a number of knots n_{knots} and a span of the transformation interval $[-B; B]$. n_{knots} controls the expressiveness of estimated density (i. e., the maximal number of modes the flow can model) and B affects the support of the transformation. In our experiments, we heuristically set $B = y_{\max} - y_{\min} + 5$, considering that the outcome is standard normalized.

For the nuisance flow, we use fully-connected subnetworks each with one hidden layer (with $h = 10$ hidden units), and the dimensionality of representation is set to $d_R = 10$.

Training. During training (see full algorithm in Appendix D), we adopt noise regularization (Rothfuss et al., 2019) and add an independent Gaussian noise $\xi_x \sim N(0, \sigma_x^2), \xi_y \sim N(0, \sigma_y^2)$ to the representation and output of the nuisance flow, i. e., $\tilde{R} = R + \xi_x; \tilde{Y} = Y + \xi_y$. For faster learning, we approximate a full-sample average $\mathbb{P}_n\{\cdot\}$ with a minibatch average $\mathbb{P}_b^{\mathcal{B}}\{\cdot\}$ for all the losses, where b is the minibatch size. We use stochastic gradient descent (SGD) for fitting the parameters of the nuisance flow, and Adam optimizer (Kingma & Ba, 2015) for the target flow with learning rates η_{N} and η_{T}, respectively. We fix the weighting hyperparameters of the loss to $\alpha = 1$ and the EMA smoothing hyperparameter to $\gamma = 0.995$.

We numerically approximate the cross-entropy and conditional cross-entropy losses via rectangle quadrature rule[14] (one-dimensional outcome) or Monte Carlo method (multi-dimensional outcome):

$$\mathcal{L}_{\text{CE}}(\beta_a) \approx \begin{cases} -h \sum_{j=1}^{K} \log g(y_j; \beta_a)\, \mathbb{P}_n\{\hat{\mathbb{P}}(Y = y_j \mid X, A = a)\}, & \text{if } d_Y = 1, \\ -\mathbb{P}_K\{\log g(\hat{Y}^a; \beta_a)\}, & \text{if } d_Y > 1, \end{cases} \tag{44}$$

$$\mathcal{L}_{\text{CCE}}(X; \beta_a) \approx \begin{cases} -h \sum_{j=1}^{K} \log g(y_j; \beta_a)\, \hat{\mathbb{P}}(Y = y_j \mid X, A = a), & \text{if } d_Y = 1, \\ -\mathbb{P}_K\{\log g(\hat{Y}^{X,a}; \beta_a)\}, & \text{if } d_Y > 1, \end{cases} \tag{45}$$

where $y_{\min} \leq y_1 < \cdots < y_K \leq y_{\max}$ is an equidistant grid of points on $\mathcal{Y}$ with step size h, $\{\hat{Y}_j^a\}_{j=1}^K$ is an i.i.d. sample drawn from $\mathbb{P}_n\{\hat{\mathbb{P}}(Y \mid X, A = a)\}$, and $\{\hat{Y}_j^{X,a}\}_{j=1}^K$ is an i.i.d. sample drawn from $\hat{\mathbb{P}}(Y \mid X, A = a)$. The grid or sample sizes, respectively, are set to $K = 100$. Both $y_{\min}$ and $y_{\max}$ are set to the empirical minimum and maximum of the train sub-sample.

Note that we would need sample splitting for training both flows to guarantee the asymptotic properties, i. e., efficiency and double robustness (see Kennedy et al., 2023, Remark 5). Nevertheless, we used all data for both components and trained our INFs with an auxiliary regularization because sample splitting can affect the performance in settings with limited data. This is consistent with previous work on deep learning for efficient treatment effect estimation (Curth & van der Schaar, 2021).

Hyperparameter tuning. We perform extensive hyperparameter tuning only for the nuisance flow. Hyperparameters for tuning include, e. g., number of knots of neural spline flows $n_{\text{knots,N}}$, the minibatch size b_{N}, the learning rate η_{N}, and the intensities of the noise regularization σ_x^2, σ_y^2. On the other hand, we discovered, that the target flow works well with the same plain set of hyperparameters in almost all the experiments. Those include the minibatch size $b_{\text{T}} = 64$ and the learning rate $\eta_{\text{T}} = 0.005$. The number of knots $n_{\text{knots,T}}$ is chosen at hand for each dataset. Further details on hyperparameter tuning are provided in Appendix G.

[14] We also experimented with the trapezoidal quadrature rule, but this did not bring any noticeable performance gain.

F. Baselines

In the following, we describe the baseline methods in detail. We use three naïve semi-parametric plug-in estimators: an extended treatment-agnostic representation network (**TARNet***) (Shalit et al., 2017), mixture density networks (**MDNs**) (Bishop, 1994) and conditional normalizing flow (**CNF**) (Trippe & Turner, 2018). Further, we use three state-of-the-art IDE baselines: kernel density estimation (**KDE**) (Kim et al., 2018), distributional kernel mean embeddings (**DKME**) (Muandet et al., 2021), and a truncated series estimator with CNF (**CNF+TS**) as suggested by (Kennedy et al., 2023).

F.1. Naïve semi-parametric plug-in estimators

Semi-parametric plug-in estimators estimate the conditional outcome distribution and perform averaging over covariates during evaluation, as introduced in Eq. (2).

TARNet*, MDNs, and CNF make use of hypernetworks (Ha et al., 2017), which take covariates X and treatment A as an input and output parameters, i. e., $\theta(X, A)$ of the estimated conditional distribution $\hat{\mathbb{P}}(Y \mid X, A)$. Hypernetwork architectures are considered to be state-of-the-art for neural conditional density estimation and can be found in, e. g., Gaussian mixtures (Bishop, 1994), variational autoencoders (Kingma & Welling, 2013), and normalizing flows (Trippe & Turner, 2018). For comparability, we use the same network structure of the nuisance flow in our INFs as the hypernetwork for the conditional distribution parameters. This gives two fully-connected subnetworks stacked on each other, i. e. FC_1 and FC_2, as introduced in Section 5.1. To regularize both conditional distribution estimators, we use noise regularization (Rothfuss et al., 2019).

TARNet*. The treatment-agnostic representation network (TARNet) (Shalit et al., 2017) was proposed to estimate nuisance parameters for CATE, i. e., conditional means of outcomes. To obtain density estimates as outputs, we report results from an extended variant which we refer to as TARNet*. Specifically, we extended the original TARNet by modeling conditional outcome distribution as a homoscedastic normal distribution. For this, we add one unconditional parameter of standard deviation, σ, so that the conditional density equals to

$$\hat{\mathbb{P}}(Y = y \mid X, A) = N(y; \mu(X, A), \sigma^2), \tag{46}$$

where $N(y; \mu, \sigma^2)$ is a density of the normal distribution, and $\mu(X, A)$ is conditional mean of outcome. Notably, we do not use the two separate outcome heads (as in the original TARNet) but only one, i. e., FC_2. This is crucial to ensure a fair comparison with other plug-in estimators. We estimate the standard deviation σ using maximum likelihood. Note also that TARNet* is restricted to normal conditional outcome distributions and thus is <u>not</u> a universal density estimator. In contrast to our INFs, TARNet* is unable to capture heavy-tailed, multi-modal, and skewed distributions.

MDNs. Mixture density networks (Bishop, 1994) are built on top of a mixture of normal distributions, and can approximate any density arbitrarily well (Titterington et al., 1985), i.e.,

$$\hat{\mathbb{P}}(Y = y \mid X, A) = \sum_{j=1}^{n_C} w_j(X, A)\, N(y; \mu_j(X, A), \sigma_j^2(X, A)) \tag{47}$$

where n_C is a number of mixture components, $w_j \geq 0, \sum_{j=1}^{n_C} w_j = 1$ are mixture weights, and $N(y; \mu_j, \sigma_j^2)$ is a density of the normal distribution. In the case of MDNs, the hypernetwork outputs logits of mixture weights and parameters of the normal distribution (i.e., mean and logarithm of the standard deviation), i. e., $\theta = \{\text{logits}(w_j), \mu_j, \log \sigma_j\}$. Here, the number of mixture components n_C controls the smoothness of the estimator and represents the main hyperparameter for tuning.

CNF. We implement conditional normalizing flow (Trippe & Turner, 2018) with the help of neural spline flows (Durkan et al., 2019). Neural spline flows construct an invertible function parameterized by θ, i. e., $f(\cdot; \theta) : \mathbb{R} \to \mathbb{R}$, which is a monotonic rational-quadratic spline with n_{knots} knots. This spline transforms the density of a base distribution on the interval $[-B; B]$. Outside of the interval, $f(\cdot)$ equals to the identity function. This allows us to perform flexible parametric density estimation with the help of the change of variables formula, i.e.,

$$\hat{\mathbb{P}}(Y = y \mid X, A) = N\Big(f^{-1}\big(y; \theta(X, A)\big); 0, 1\Big) \left| \frac{\mathrm{d}f}{\mathrm{d}Y}\big(f^{-1}(y; \theta(X, A))\big) \right|^{-1} \tag{48}$$

where $f^{-1}(\cdot; \theta)$ is the inverse transformation, and the density of standard normal distribution $N(y; 0, 1)$ serves as a base distribution. As already discussed in Appendix E, B affects the support of transformation, and the number of knots n_{knots} controls the flexibility of the estimator and represents the main hyperparameter for tuning.

F.2. Kernel density estimation (KDE)

Kernel density estimation (KDE) is a semi-parametric method for IDE (Kim et al., 2018). It builds upon the idea of a density functional, namely $T_y(Y; h_a)$, to transform a random variable Y into a proper density via

$$T_y(Y; h_a) = \frac{1}{h_a} K\left(\frac{\|Y - y\|_2}{h_a}\right) = \frac{1}{h_a\sqrt{2\pi}} \exp\left(-\frac{\|Y - y\|_2^2}{2h_a^2}\right), \tag{49}$$

where $K(x) = \frac{1}{\sqrt{2\pi}} \exp(-x^2/2)$ is a radial basis function (RBF) with a treatment-specific smoothing parameter h_a called bandwidth, and $\|\cdot\|_2$ is the L_2-norm.

Robins & Rotnitzky (2001) proposed a semi-parametric plug-in estimator of the interventional density

$$\hat{\mathbb{P}}^{\text{PI}}(Y[a] = y) = \mathbb{P}_n\Big\{\hat{\mathbb{E}}\big(T_y(Y; h_a) \mid X, A = a\big)\Big\}, \tag{50}$$

where $\hat{\mu}_{a,y}(X) = \hat{\mathbb{E}}\big(T_y(Y; h_a) \mid X, A = a\big)$ is a functional regression of X and A on $T_y(Y; h_a)$. Kim et al. (2018) further extended this estimator to an A-IPTW-style semi-parametric estimator

$$\hat{\mathbb{P}}^{\text{A-IPTW}}(Y[a] = y) = \mathbb{P}_n\left\{\frac{\mathbb{1}(A = a)}{\hat{\pi}_a(X)}\Big(T_y(Y; h_a) - \hat{\mu}_{a,y}(X)\Big) + \hat{\mu}_{a,y}(X)\right\}, \tag{51}$$

where $\hat{\pi}_a(X)$ is an estimator of the propensity score. This estimator is efficient with respect to the L_1 distance between two interventional distributions.

The main challenge here is building a functional regression $\hat{\mu}_{a,y}(X)$. Unfortunately, the work by Kim et al. (2018) does not provide effective, practical solutions. Even more so, Eq. (51) does not guarantee that the estimated density is proper, i. e., integrates to 1 and is positive, especially in a small sample regime or when the propensity score has extremely low values.

To estimate the nuisance parameters, namely, the propensity score and the functional regression, we use the same network structure as for the nuisance flow of our INFs (see Section 5.1). In this way, we estimate the propensity score and perform a functional regression with two joined, fully-connected subnetworks (i.e., FC_1 and FC_2). The first subnetwork, FC_1, outputs a representation R and estimates the propensity score. The second subnetwork, FC_2, then takes the representation R and the treatment A, and performs an outcome regression: $\hat{Y} = \hat{\mathbb{E}}(Y \mid X, A)$. The functional expression, i. e., Eq. (49), is predicted via $\hat{\mu}_{a,y}(X) = T_y(\hat{\mathbb{E}}(Y \mid X, A); h_a)$. Although, this is a biased estimator of $\mu_{a,y}(X)$, it ensures a proper normalization, i.e., $\int_{\mathcal{Y}} \hat{\mu}_{a,y}(X)\,\mathrm{d}y = 1$.

To fit FC_1 and FC_2, we use the sum of mean-squared error ($\mathcal{L}_{\text{MSE}}$) and binary cross-entropy ($\mathcal{L}_\pi$) losses via

$$\mathcal{L}_{\text{KDE}}(\hat{\mathbb{E}}, \hat{\pi}_a) = \mathbb{P}_n\{\mathcal{L}_{\text{MSE}} + \alpha\mathcal{L}_\pi\} \text{ with } \mathcal{L}_{\text{MSE}} = (\hat{Y} - Y)^2; \quad \mathcal{L}_\pi = \text{BCE}(\hat{\pi}_A(X), A), \tag{52}$$

where α is a hyperparameter. In our experiments, we set $\alpha = 1$ and fit the nuisance parameters (i.e., $\hat{\pi}_a$ and $\hat{\mathbb{E}}(Y \mid X, A)$) using the Adam optimizer with $n_{\text{iter}} = 10000$ iterations. Both learning rate η and minibatch size b are subject to hyperparameter tuning.

We employ a median heuristic (Garreau et al., 2017) for choosing the bandwidth h_a, i.e.,

$$h_a^{\text{med}} = \sqrt{\frac{1}{2}\,\text{Median}\left(\|Y_i - Y_j\|_2^2 \mid A = a\right)}, \quad 1 \le i < j \le n, \tag{53}$$

where $\|\cdot\|_2$ is the L_2-norm, and where Y_i, Y_j are observations from the train subset, conditioned on $A = a$. To address the numeric instability of the A-IPTW estimator, we discard observations with too small propensity scores ($\hat{\pi}_a(X) < 0.05$) from averaging in Eq. (51), similarly to our INFs.

F.3. Distributional kernel mean embeddings (DKME)

Distributional kernel mean embeddings (DKME) (Muandet et al., 2021) is a non-parametric plug-in estimator of interventional densities. This method builds a kernel mean embedding (KME), namely, $\mu_{Y|X,A=a}$, for the conditional distribution $\mathbb{P}(Y \mid X, A = a)$ via

$$\mu_{Y|X,A=a}(y) \coloneqq \mathop{\mathbb{E}}_{Y \sim \mathbb{P}(Y|X,A=a)} l_a(y, Y), \tag{54}$$

where $l_a(\cdot,\cdot)$ is a measurable positive definite kernel associated with a reproducing kernel Hilbert space $\mathcal{H}$, so that $\mu_{Y|X,A=a}$ provides a mapping from the space of conditional distributions to the space of functions $\mathcal{H}$. If $l_a(\cdot,\cdot)$ is properly normalized, then $\mu_{Y|X,A=a}(y)$ is in fact a conditional density estimator.

To estimate the KME of the conditional outcome distribution (conditional mean embedding), we use the i.i.d. sample $\mathcal{D} = \{X_i, A_i, Y_i\}_{i=1}^n$, and split it into control and treated subsamples: $\mathcal{D} = \{X_i^0, Y_i^0\}_{i=1}^{n_0} \cup \{X_i^1, Y_i^1\}_{i=1}^{n_1}$. Then, $\mu_{Y|X,A=a}$ can be estimated via

$$\hat{\mu}_{Y|X,A=a}(y) = \sum_{i=1}^{n_a} w_i^a(X)\, l_a(y, Y_i^a), \tag{55}$$

$$\big(w_1^a(X), \dots, w_{n_a}^a(X)\big)^\intercal = (\mathbf{K}^a + n_a\varepsilon\mathbf{I})^{-1}\,\mathbf{k}^a(X) \in \mathbb{R}^{n_a}, \tag{56}$$

$$\mathbf{k}^a(X) = \big(k(X, X_1^a), \dots, k(X, X_{n_a}^a)\big)^\intercal \in \mathbb{R}^{n_a}, \tag{57}$$

where $\mathbf{I} \in \mathbb{R}^{n_a \times n_a}$ is an identity matrix, $\varepsilon > 0$ is a regularization hyperparameter, $\mathbf{K}^a \in \mathbb{R}^{n_a \times n_a}$ is a kernel matrix with elements $\mathbf{K}_{ij}^a = k(X_i^a, X_j^a)$, and $k(\cdot,\cdot)$ is a second kernel representing conditional dependencies between X and Y (Grünewälder et al., 2012).

Muandet et al. (2021) further developed a KME for interventional distribution, i. e., $\mu_{Y[a]}$, and its empirical estimate, $\hat{\mu}_{Y[a]}$:

$$\mu_{Y[a]}(y) = \mathop{\mathbb{E}}_{X\sim\mathbb{P}(X)} \mu_{Y|X,A=a}(y) \tag{58}$$

$$\hat{\mu}_{Y[a]}(y) = \mathbb{P}_n\{\hat{\mu}_{Y|X,A=a}(y)\} = \sum_{i=1}^{n_a} \beta_i^a\, l_a(y, Y_i^a), \tag{59}$$

$$(\beta_1^a, \dots, \beta_{n_a}^a)^\intercal = (\mathbf{K}^a + n_a\varepsilon\mathbf{I})^{-1}\,\tilde{\mathbf{K}}^a\,\mathbf{1}_m \in \mathbb{R}^{n_a}, \tag{60}$$

where $\tilde{\mathbf{K}}^a \in \mathbb{R}^{n_a \times n}$ is a kernel matrix with elements $\tilde{\mathbf{K}}_{ij}^a = k(X_i^a, X_j)$, and $\mathbf{1}_m = (1/n, \dots, 1/n)^\intercal$.

For our experiments, we choose both kernels, i. e., outcome kernel, $l_a(\cdot,\cdot)$, and conditional kernel, $k(\cdot,\cdot)$, to be RBF kernels with bandwidth parameters $h_{a,l}$ and h_k, respectively. Therefore, $\hat{\mu}_{Y[a]}(y)$ represents a valid interventional density estimator. Nevertheless, due to small sample sizes, some β_i^a could be negative and the estimated density ends up having negative values.

We set the bandwidth of the outcome kernel, $h_{a,l}$ according to the median heuristic from Eq. (53). The bandwidth of the conditional kernel h_k and the regularization hyperparameter ε are subjects to the hyperparameter tuning. Motivated by the interpretation of conditional mean embedding as kernel ridge regression (Grünewälder et al., 2012), we use out-sample MSE of the ridge regression with parameters h_k and ε as a tuning criterion.

F.4. Truncated series estimator with CNF (CNF+TS)

The truncated series (TS) estimator (Efromovich, 2010) is a fully-parametric estimator, which is used as a second-step model in (Kennedy et al., 2023). The parametric density model uses so-called orthogonal basis functions $b(y) = \{b_j(y)\}_{j=1}^d$ and is parameterized by the set of parameters $\beta \in \mathbb{R}^d$:

$$g(y;\beta) = q(y) + \sum_{j=1}^{d} \beta_j b_j(y), \tag{61}$$

where $q(y)$ is some fixed density (e. g., uniform) d is the basis dimensionality, and $\int_{\mathcal{Y}} b_j(y)\,\mathrm{d}y = 0$. $g(y;\beta)$ is also called a projection onto the orthogonal basis. This density estimator also naturally extends to higher dimensions. For example, a two-dimensional density estimation thus yields

$$g(y;\beta) = q(y) + \sum_{j=1}^{d}\sum_{k=1}^{d} \beta_{jk} b_j(y_1) b_k(y_2), \tag{62}$$

where $\beta \in \mathbb{R}^{d\times d}$ is a parameters tensor and $b(y) = \{b_j(y_1)b_k(y_2)\}_{j,k=1}^d$.

Following (Kennedy et al., 2023), we bound the support of Y to $[0, 1]$, set $q(y) = 1$, and take $b(y)$ as cosine basis:

$$b_j(y) = \sqrt{2}\cos(\pi j y), \tag{63}$$

which satisfies $\int_0^1 b_j(y)\,\mathrm{d}y = 0$.

The estimation of IDE projection parameters is done differently from INFs. Specifically, truncated series estimator aims to minimize L_2 distance, but not KL-divergence via

$$\hat{\beta}_a = \arg\min_{\beta_a} \int_{\mathcal{Y}} \left(g(y; \beta_a) - \mathbb{P}(Y[a] = y)\right)^2 \mathrm{d}y. \tag{64}$$

In the case of Y having support $[0, 1]$ and $q(y) = 1$, the projection parameters have a closed form solution

$$\hat{\beta}_a = \mathop{\mathbb{E}}_{Y^a \sim \mathbb{P}(Y[a])} \big(b(Y^a)\big). \tag{65}$$

Kennedy et al. (2023) proposed an efficient estimator of the L_2 projection parameters via one-step bias correction

$$\hat{\beta}_a^{\text{A-IPTW}} = \mathbb{P}_n \left\{ \frac{\mathbb{1}(A = a)}{\hat{\pi}_a(X)} \Big(b(Y) - \hat{\mu}_a(X) \Big) + \hat{\mu}_a(X) \right\}, \tag{66}$$

where $\hat{\pi}_a(X)$ is an estimator of the propensity score and $\hat{\mu}_a(X) = \hat{\mathbb{E}}(b(Y) \mid X, A = a)$ is a functional regression of X and A on $b(Y)$.

In our experiments, we fit the truncated series together with CNF, which was also done in (Kennedy et al., 2023), but with a different conditional density estimator. Then, $\hat{\mu}_a(X)$ can be approximated via

$$\hat{\mu}_a(X) \approx \begin{cases} h \sum_{j=1}^{K} b(y)\, \hat{\mathbb{P}}(Y = y_j \mid X, A = a), & \text{if } d_Y = 1, \\ \mathbb{P}_K\{b(\hat{Y}^{X,a})\}, & \text{if } d_Y > 1, \end{cases} \tag{67}$$

where $\hat{\mathbb{P}}(Y \mid X, A = a)$ is conditional distribution, modeled by CNF, $y_{\min} \leq y_1 < \cdots < y_K \leq y_{\max}$ is an equidistant grid of points on $\mathcal{Y}$ with step size h, and $\{\hat{Y}_j^{X,a}\}_{j=1}^K$ is an i.i.d. sample drawn from $\hat{\mathbb{P}}(Y \mid X, A = a)$. The grid (or sample sizes) are set to $K = 100$ (the same, as for INFs).

Importantly, the density $g(y; \beta_a)$ is not guaranteed to be positive and post-hoc re-normalization is required in finite-sample estimation (Efromovich, 2010). Such issues cannot be addressed by, e. g., tuning the basis dimensionality, d. Specifically, by setting it too low, the density estimator will be underfitting; by setting it too high, it struggles with negative values due to heavy tails or low-density regions. For details on choosing d, we refer to Appendix G.

G. Hyperparameter tuning

We performed hyperparameters tuning of the nuisance parameters models for all the baselines based on five-fold cross-validation using the train subset. For each baseline, we performed a grid search with respect to different tuning criteria, evaluated on the validation subsets. Table 5 shows grids for hyperparameter tuning and other parameters, such as tuning criteria, number of training iterations, and optimizers. We aimed for a fair comparison and thus kept the number of parameters, network structures, and grid size similar across models. For the sake of reproducibility, we make the chosen hyperparameters for all the experiments public (see YAML files in our GitHub[15]).

Importantly, to facilitate the convergence of baseline methods, we additionally perform a standard normalization of both factual and counterfactual outcomes for all the datasets.

For the second-step models, e. g., (i) the target flow of INFs and (ii) truncated series of CNF+TS, we did not perform tuning but instead proceeded as follows. For (i), we heuristically set the number of knots of the target flow, $n_{\text{knots,T}}$, to the optimal number of knots of the nuisance flow. We observed that this is the only important hyperparameter, as it controls the expressiveness of the estimator. For (ii), tuning the main hyperparameter, i. e., the basis dimensionality, d, had a major negative side-effect. It resulted in either underfitting the density (for too small d) or negative density values due to too high flexibility (for large d). As a remedy, we set $d = 10$ in all the experiments.

[15] https://anonymous.4open.science/r/AnonymousInterFlow-E2F3

Table 5. Hyperparameter tuning for baselines.

Model	Sub-model	Hyperparameter	Range / Value
TARNet*	—	Intensity of noise regularization (σ_x^2)	0.0, 0.01^2, 0.05^2, 0.1^2
		Intensity of noise regularization (σ_y^2)	0.0, 0.01^2, 0.05^2, 0.1^2
		Learning rate (η)	0.001, 0.005
		Minibatch size (b)	32, 64
		Tuning strategy	random grid search with 50 runs
		Tuning criterion	$\mathcal{L}_{\text{NLL}}$
		Number of train iterations (n_{iter})	5000
		Optimizer	SGD (momentum = 0.9)
MDNs	—	Number of mixture components (n_C)	5, 10, 20
		Intensity of noise regularization (σ_x^2)	0.0, 0.01^2, 0.05^2, 0.1^2
		Intensity of noise regularization (σ_y^2)	0.0, 0.01^2, 0.05^2, 0.1^2
		Learning rate (η)	0.001, 0.005
		Minibatch size (b)	32, 64
		Tuning strategy	random grid search with 50 runs
		Tuning criterion	$\mathcal{L}_{\text{NLL}}$
		Number of train iterations (n_{iter})	5000
		Optimizer	SGD (momentum = 0.9)
KDE	—	Learning rate (η)	0.001, 0.005, 0.1
		Minibatch size (b)	32, 64, 128
		Tuning strategy	full grid search
		Tuning criterion	$\mathcal{L}_{\text{MSE}} + \alpha\mathcal{L}_\pi$
		Number of train iterations (n_{iter})	10000
		Optimizer	Adam (betas=(0.9, 0.999))
DKME	—	Kernel smoothness ($\sigma_k = 2h_k^2$)	0.0001, 0.001, 0.01, 0.1, 1, 10, 20
		Regularization parameter (ε)	0.0001, 0.001, 0.01, 0.1, 1, 10
		Tuning strategy	full grid search
		Tuning criterion	MSE of ridge regression
CNF+TS	CNF	Same as INFs/ nuisance flow ($\hat{=}$ CNF)	
	TS	Basis dimensionality (d)	10
		Tuning strategy	w/o tuning
INFs	nuisance flow ($\hat{=}$ CNF)	Number of knots ($n_{\text{knots,N}}$)	5, 10, 20
		Intensity of noise regularization (σ_x^2)	0.0, 0.01^2, 0.05^2, 0.1^2
		Intensity of noise regularization (σ_y^2)	0.0, 0.01^2, 0.05^2, 0.1^2
		Learning rate (η_{N})	0.001, 0.005
		Minibatch size (b_{N})	32, 64
		Tuning strategy	random grid search with 50 runs
		Tuning criterion	$\mathcal{L}_{\text{NLL}}$
		Number of train iterations ($n_{\text{iter,N}}$)	5000
		Optimizer	SGD (momentum = 0.9)
	target flow	Number of knots ($n_{\text{knots,T}}$)	dataset specific*
		Learning rate (η_{T})	0.005
		Minibatch size (b_{T})	64
		Tuning strategy	w/o tuning
		Number of train iterations ($n_{\text{iter,T}}$)	4000
		Optimizer	Adam (betas=(0.9, 0.999))

* $n_{\text{knots,T}} = 5$ (synthetic data), $= 10$ (IHDP, HC-MNIST datasets), $= n_{\text{knots,N}}$ (ACIC 2016 & 2018 datasets)

H. Dataset details

H.1. Synthetic dataset

We sample $n = 1000$ observations from the SCM (Fig. 1) and use a ten-fold split for train/test samples (90%/10%). We separately perform hyperparameter tuning based on the first split for each baseline and each level b. We then report an average out-sample log-likelihood over ten folds.

H.2. IHDP dataset

The IHDP dataset (Hill, 2011) uses a real-world dataset with 25 covariates (6 continuous, 19 binary) and one binary treatment, capturing aspects related to children and their mothers. Both treated and untreated, synthetic outcomes of IHDP are sampled from different conditional normal distributions. These distributions are homoscedastic ($\sigma^2 = 1$) but have substantially different conditional means. We used the setting "B" in (Hill, 2011) with a following data generating mechanism:

$$\begin{cases} X \sim \text{Real-World}(\cdot), \\ A \sim \text{Real-World}(X), \\ Y \sim N\big(A\,(X\beta - \omega) + (1-A)\,(\exp((X+W)\beta)), 1\big), \end{cases} \tag{68}$$

where β, W, ω are constant parameters of the simulation. For further details, we refer to (Hill, 2011).

H.3. ACIC 2016 & 2018 datasets

Covariates of ACIC 2016 are taken from a large study of developmental disorders (Niswander, 1972), and covariates of ACIC 2018 are derived from the linked birth and infant death data (MacDorman & Atkinson, 1998). ACIC 2016 and ACIC 2018 differ in the number of true confounders, the varying level of overlap, and the form of conditional outcome distributions. ACIC 2016 has 77 different data-generating mechanisms with 100 equal-sized samples for each mechanism ($n = 4802, d_X = 82$).[16] ACIC 2018 provides 63 distinct data-generating mechanisms with around 40 non-equal-sized samples for each mechanism (n ranges from $1,000$ to $50,000$, $d_X = 177$). Notably, ACIC 2018 has a constant CATE for most of the datasets, but heterogeneous propensity scores.

H.4. HC-MNIST

Jesson et al. (2021) introduced a complex high-dimensional, semi-synthetic dataset based on the MNIST image dataset LeCun (1998), namely HC-MNIST. This dataset maps high-dimensional images onto a one-dimensional manifold, where potential outcomes depend in a complex way on the average intensity of light and the label of an image. The treatment also uses this one-dimensional summary, ϕ, together with an additional (hidden) synthetic confounder, U. This is described by the following data-generating mechanism:

$$\begin{cases} U \sim \text{Bern}(0.5), \\ X \sim \text{MNIST-image}(\cdot), \\ \phi := \left(\text{clip}\left(\frac{\mu_{N_x} - \mu_c}{\sigma_c}; -1.4, 1.4\right) - \text{Min}_c\right) \frac{\text{Max}_c - \text{Min}_c}{1.4 - (-1.4)}, \\ \alpha(\phi; \Gamma^*) := \frac{1}{\Gamma^* \,\text{sigmoid}(0.75\phi + 0.5)} + 1 - \frac{1}{\Gamma^*}, \\ \beta(\phi; \Gamma^*) := \frac{\Gamma^*}{\text{sigmoid}(0.75\phi + 0.5)} + 1 - \Gamma^*, \\ A \sim \text{Bern}\left(\frac{u}{\alpha(\phi;\Gamma^*)} + \frac{1-u}{\beta(\phi;\Gamma^*)}\right), \\ Y \sim N\big((2A-1)\phi + (2A-1) - 2\sin(2(2A-1)\phi) - 2(2u-1)(1+0.5\phi), 1\big), \end{cases} \tag{69}$$

where c is a label of the digit from the sampled image X; μ_{N_x} is the average intensity of the sampled image; μ_c and σ_c are the mean and standard deviation of the average intensities of the images with the label c; and $\text{Min}_c = -2 + \frac{4}{10}c, \text{Max}_c = -2 + \frac{4}{10}(c+1)$. The parameter Γ^* defines what factor influences the treatment assignment to a larger extent, i.e., the additional confounder or the one-dimensional summary. We set $\Gamma^* = \exp(1)$. For further details, we refer to (Jesson et al., 2021).

[16] After one-hot-encoding of categorical covariates.

For the experiments with HC-MNIST, we use a larger network size for our INFs (compared to other benchmarking experiments) to allow for more flexibility. We set the number of hidden units in fully-connected subnetworks to $h = 30$, and the dimensionality of representation $d_R = 30$. We also increase the number of training iterations to $n_{\text{iter,N}} = 15,000$ and $n_{\text{iter,T}} = 5000$.

Fig. 5 shows both ground-truth interventional, $\mathbb{P}(Y[a])$, and observational, $\mathbb{P}(Y \mid A = a)$, distributions together with our INFs A-IPTW estimator, $\hat{\mathbb{P}}^{\text{INFs}}(Y[a])$. Remarkably, the interventional distributions in HC-MNIST are multi-modal and differ a lot from observational distributions.

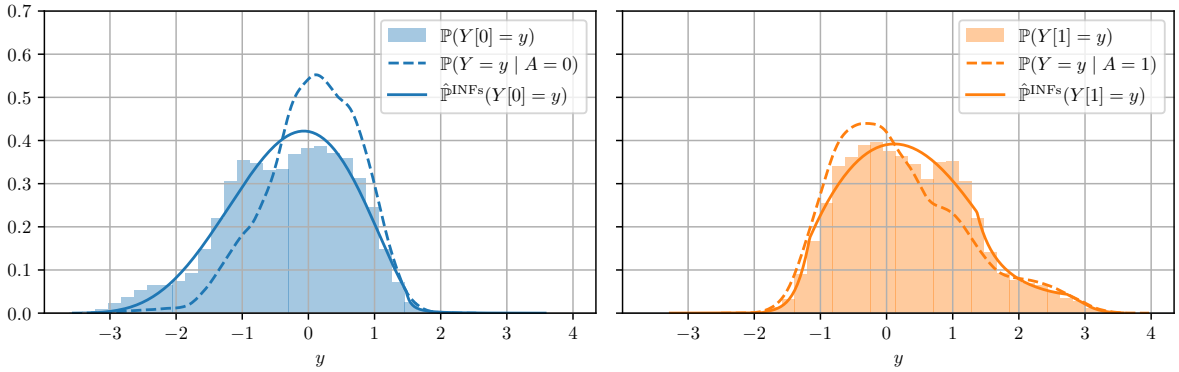

Figure 5. Empirical ground-truth interventional and conditional distributions of the HC-MNIST synthetic outcome. We also plot our INFs density estimator, i. e., $\hat{\mathbb{P}}^{\text{INFs}}(Y[a])$.

I. Synthetic two-dimensional data

In the following, we benchmark our INFs for estimating an interventional density of the multidimensional outcome, $d_Y = 2$.

Noisy moons synthetic data. We used a standard two-dimensional toy data generator, namely moons data.[17] It draws samples from two interleaving half-circles with different noise levels ε. The noise level controls the level of the overlap between two half-circles (a higher σ corresponds to a better overlap, and, thus, a satisfaction of the positivity assumption). We draw $n = 1000$ observations of two-dimensional covariates, i. e., $d_X = 2$, and use an inclusion to the top or bottom semi-circle as a treatment. Finally, we generate the synthetic outcome by rotating the covariates by a random treatment-specific angle, i. e., α_0 and α_1:

$$\begin{cases} X, A \sim \text{Make-Moons}(\cdot, \sigma), \\ \varepsilon \sim N(0, 0.1^2), \\ \alpha_0 = \frac{\pi}{4} + \varepsilon, \quad \alpha_0 = -\frac{\pi}{4} + \varepsilon, \\ Y := R(\alpha_1 A + \alpha_0 (1 - A))X + \varepsilon \mathbf{1}_2, \end{cases} \tag{70}$$

where $\mathbf{1}_2 = (1, 1)^T$, and $R(\alpha) = \begin{pmatrix} \cos\alpha & -\sin\alpha \\ \sin\alpha & \cos\alpha \end{pmatrix}$ is an α-angle rotation matrix. We set $\sigma = 0.75$.

For the benchmarking with the noisy moons data, we increased the number of the training iterations for all the plug-in methods ($n_{\text{iter}} = 10000$) and for our INFs, ($n_{\text{iter,N}} = 10000, n_{\text{iter,T}} = 5000$). To model two-dimensional (conditional) density, we employed an auto-regressive extension of neural spline flows (Dolatabadi et al., 2020). We decreased the number of sampled points for approximating the cross-entropy, $K = 70$, to speed up the training, and set the number of knots for the target flow to $n_{\text{knots,T}} = 5$. As the truncated series estimator of CNF+TS requires large amounts of training data in high-dimensional density estimation, we reduce the basis dimensionality to $d = 5$.

Results. Table 6 shows the results. Here, our INFs (main) scores second best in terms of in-sample performance, but, more importantly, best in out-sample performance. MDNs, although scoring the best with in-sample average log-probability, do not generalize well. Finally, we again confirmed, that our INFs are superior over their ablations and other existing methods, e.g., KDE and DKME. We also see that CNF+TS performs the worst, confirming that truncated series do not scale well to higher dimensions.

Table 6. Results for synthetic experiments using the noisy moons synthetic data. The performance is benchmarked using the empirical in-sample / out-sample average log-probability for the two potential outcomes (i.e., $a = 0$ and $a = 1$). Reported: mean $\pm$ standard deviation over ten-fold train-test splits.

	$a = 0$		$a = 1$	
	log-prob$_{\text{in}}$	log-prob$_{\text{out}}$	log-prob$_{\text{in}}$	log-prob$_{\text{out}}$
TARNet*	-2.907 ± 0.121	-3.005 ± 0.263	-2.781 ± 0.092	-2.955 ± 0.222
MDNs	$\mathbf{-2.698 \pm 0.050}$	-2.887 ± 0.173	$\mathbf{-2.683 \pm 0.051}$	-2.827 ± 0.165
CNF [$\hat{=}$ INFs w/o target flow]	-2.767 ± 0.087	-2.935 ± 0.239	-2.807 ± 0.162	-2.900 ± 0.183
KDE (Kim et al., 2018)	-2.913 ± 0.015	-2.916 ± 0.052	-2.898 ± 0.013	-2.901 ± 0.049
DKME (Muandet et al., 2021)	-2.872 ± 0.016	-2.875 ± 0.056	-2.847 ± 0.012	-2.849 ± 0.067
CNF+TS (Kennedy et al., 2023)	-3.803 ± 0.067	-3.879 ± 0.329	-4.095 ± 0.148	-4.255 ± 0.503
INFs w/o bias corr	-2.787 ± 0.057	$\underline{-2.794 \pm 0.130}$	-2.785 ± 0.048	$\underline{-2.788 \pm 0.135}$
INFs (main)	$\underline{-2.764 \pm 0.030}$	$\mathbf{-2.766 \pm 0.102}$	$\underline{-2.780 \pm 0.022}$	$\mathbf{-2.785 \pm 0.134}$

Higher = better (best in bold, second best underlined)

[17] https://scikit-learn.org/stable/modules/generated/sklearn.datasets.make_moons.html

J. Additional results

J.1. IHDP dataset

Here, we provide additional results for the IHDP dataset with an alternative evaluation metric, that is, the empirical Wasserstein distance.

Evaluation metric. For one-dimensional outcomes, the Wasserstein distance between two distributions can be simply expressed via quantile functions

$$W^p(\mathbb{P}_1, \mathbb{P}_2) = \left(\int_0^1 |\mathbb{F}_1^{-1}(q) - \mathbb{F}_2^{-1}(q)|^p \, \mathrm{d}q \right)^{1/p}, \tag{71}$$

where $\mathbb{F}_1^{-1}(q)$ and $\mathbb{F}_2^{-1}(q)$ are quantile functions of $\mathbb{P}_1$ and $\mathbb{P}_2$, respectively. The Wasserstein distance is not upper-bounded and equals zero if and only if both distributions are the same. Here, we compute the empirical Wasserstein distance, i. e., $\hat{W}^1$, based on empirical quantile functions. This requires two samples: one from the ground-truth interventional distribution and another from the estimated density. Therefore, methods which do not provide proper density and, specifically, direct sampling (e. g., KDE, DKME, and CNF+TS) cannot be used for evaluation.

Table 7 shows the results. Note that TARNet* is the plug-in with the ground-truth conditional density estimator for this specific dataset, due to the fact of how the data was constructed. Hence, we do not consider TARNet* as a baseline but rather interpret it as a bound for the best performance. We see that all baselines (MDNs, CNF, INFs w/o bias correction) are inferior by a large margin. In contrast, our INFs achieve a performance similar to the bound. In particular, our INFs perform overall best: our INFs are superior over the two other naïve plug-in estimators and the variant of INFs without bias correction. In sum, the results corroborate our findings from the main paper and add to the effectiveness of our INFs.

Table 7. Additional results for semi-synthetic experiments using the IHDP dataset. The performance is benchmarked using the empirical in-sample / out-sample Wasserstein distance (i.e., $\hat{W}^1_{\text{in}}$ and $\hat{W}^1_{\text{out}}$) for the two potential outcomes (i.e., $a = 0$ and $a = 1$). Reported: mean $\pm$ standard deviation over ten-fold train-test splits.

	$a = 0$		$a = 1$	
	$\hat{W}^1_{\text{in}}$	$\hat{W}^1_{\text{out}}$	$\hat{W}^1_{\text{in}}$	$\hat{W}^1_{\text{out}}$
TARNet* [$\hat{=}$ ground-truth for IHDP]	<u>0.048 ± 0.014</u>	**0.131 ± 0.040**	**0.046 ± 0.024**	<u>0.126 ± 0.065</u>
MDNs	0.067 ± 0.053	0.156 ± 0.054	0.121 ± 0.076	0.183 ± 0.071
CNF [$\hat{=}$ INFs w/o target flow]	0.118 ± 0.048	0.192 ± 0.069	0.111 ± 0.087	0.146 ± 0.082
INFs w/o bias corr	0.075 ± 0.030	0.137 ± 0.051	0.107 ± 0.060	0.128 ± 0.057
INFs (main)	**0.040 ± 0.009**	<u>0.132 ± 0.051</u>	<u>0.100 ± 0.037</u>	**0.117 ± 0.055**

Higher = better (best in bold, second best underlined)

J.2. ACIC 2016 & 2018 datasets

In the following, we present detailed results of the experiments with ACIC 2016 and ACIC 2018 datasets. Fig. 6 reports the median performance for the individual datasets in ACIC 2016, and Fig. 7 for ACIC 2018. In the latter, datasets are grouped by sample size. We also show the performance gain of our INFs (when INFs score better than the baselines). The percentage of the datasets with the positive performance gain for our INFs roughly corresponds to the percentage reported in the Table 3. For ACIC 2016, our INFs are the best method for 30 + 19 = 49 out of 2 * 77 = 154 potential outcomes of individual datasets (32%) with respect to out-of-sample average log-probability. For comparison, the second-best baseline (MDNs) are only best for 22 + 24 = 46 out of 2 * 77 potential outcomes of individual datasets (30%), and thus inferior. For ACIC 2018, our INFs are the best method for 8 + 9 = 17 out of 2 * 24 potential outcomes of individual datasets (35%). For comparison, the second-best baseline (also MDNs) is only best for 5 + 4 = 9 out of 2 * 24 potential outcomes of individual datasets (19%), and thus again inferior. This thus provides consistent performance that our INFs are highly effective.

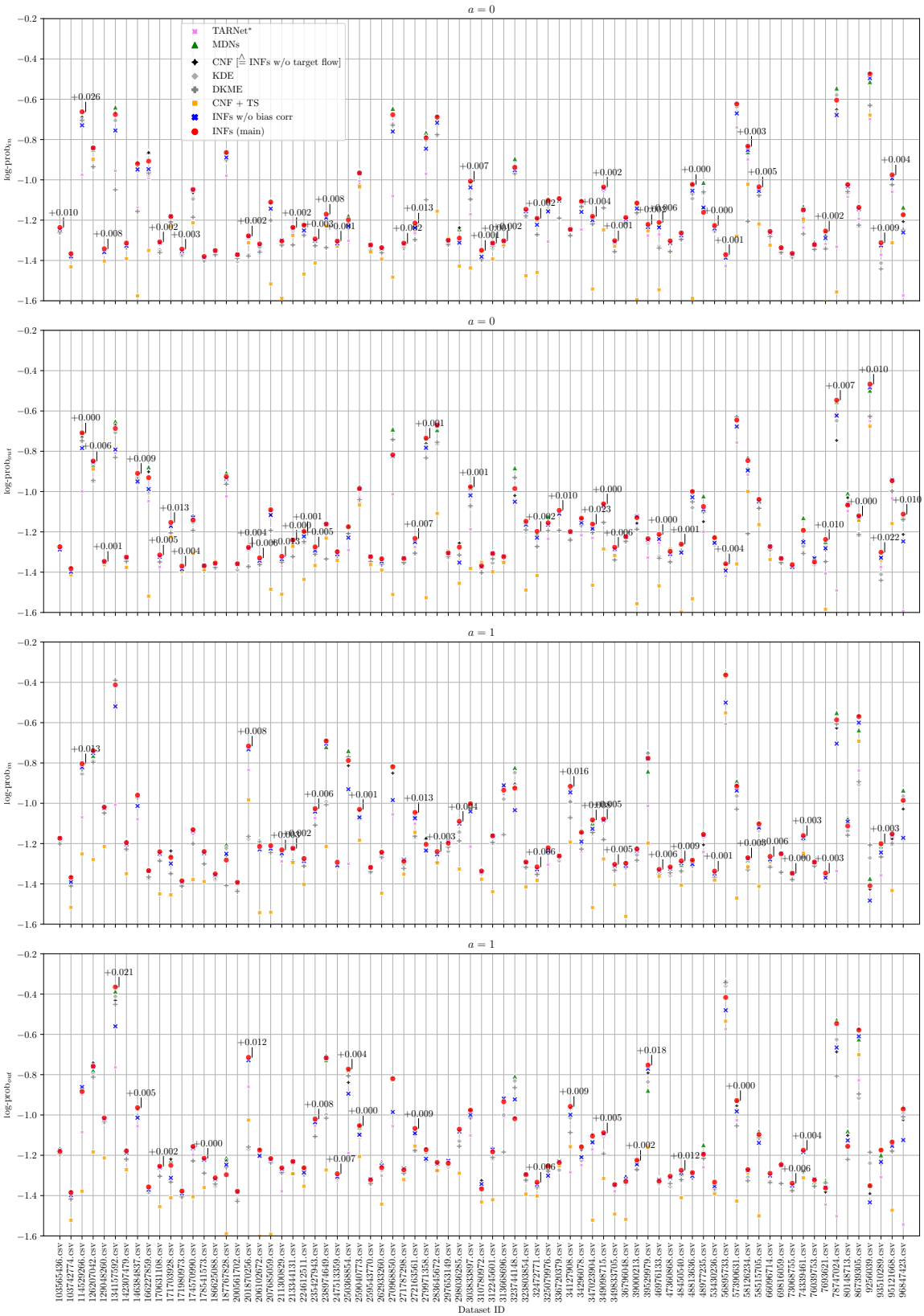

Figure 6. Detailed results for ACIC 2016. For each dataset, we perform five random train-test splits, tune the baselines on the first split, and evaluate the average in-sample / out-sample log-probability for each of the two potential outcomes separately. Shown: median over five runs and improvement of our INFs (main), when they score better than other baselines.

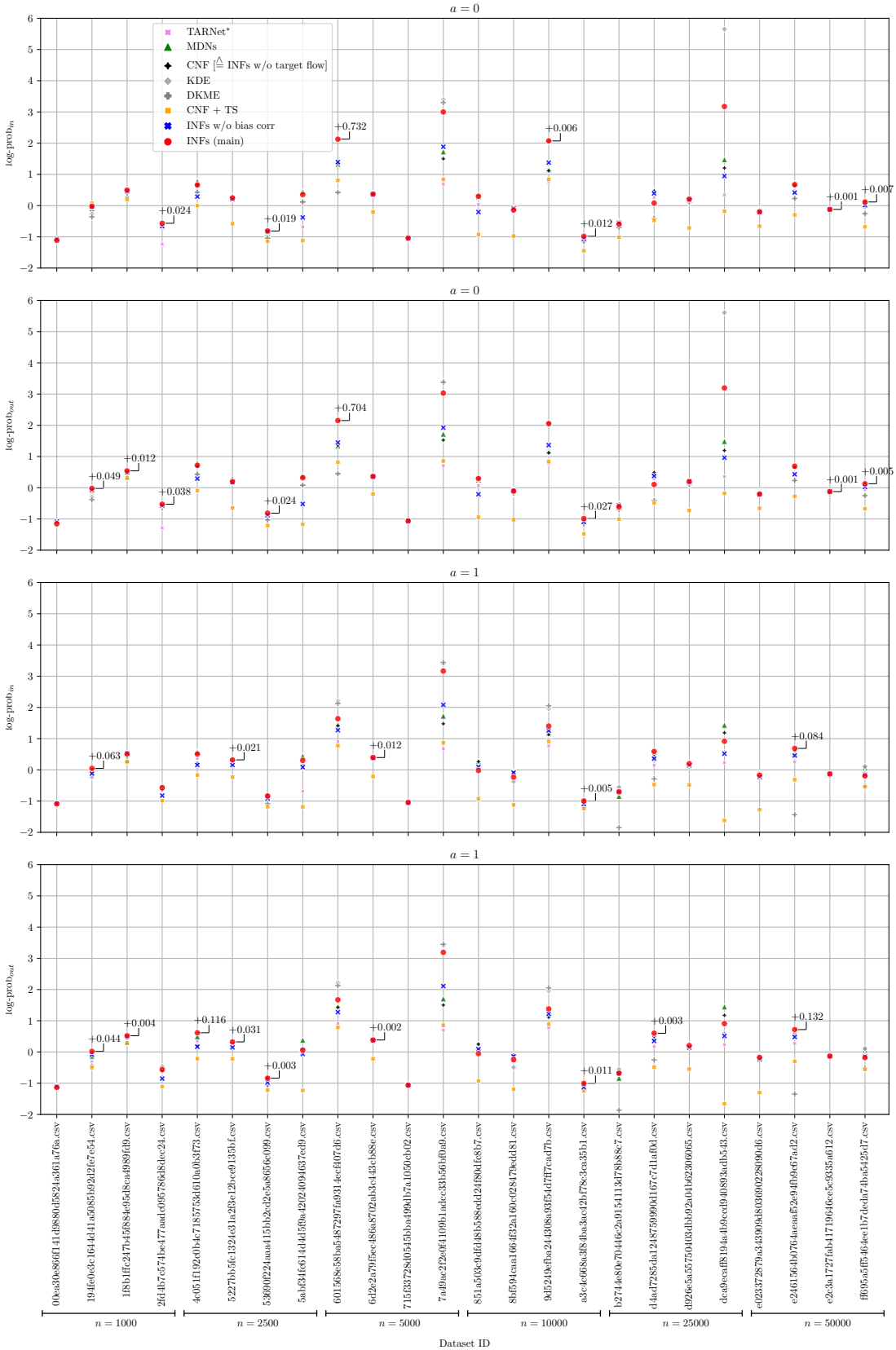

Figure 7. Detailed results for ACIC 2018, sorted with respect to sample sizes. For each dataset, we perform five random train-test splits, tune the baselines on the first split, and evaluate the average in-sample / out-sample log-probability for each of the two potential outcomes separately. Shown: median over five runs and improvement of our INFs (main), when they score better than other baselines.

K. Qualitative insights

In the following, we qualitatively inspect situations where our INFs fail to better understand their strengths and limitations. We base our qualitative analysis on the ACIC 2016 & 2018 datasets. Figure 8 showcases five specific datasets, where our INFs scored worst or second worst in comparison to the other baselines. We observe that INFs tend to struggle for datasets with outliers (e.g., 48977235.csv, 206102672.csv); for datasets that include a combination of heavy tails and multiple modes (e.g., 6d2e2a79f5ec486a8702ab3c443cb88e.csv, 851a503c9dfd48b588edd24f80dfc8b7.csv); and over-parametrization of the target flow, i.e., misspecified number of knots, $n_{\text{knots,T}}$ (e.g., 00ea30e866f141d9880d5824a361a76a.csv).

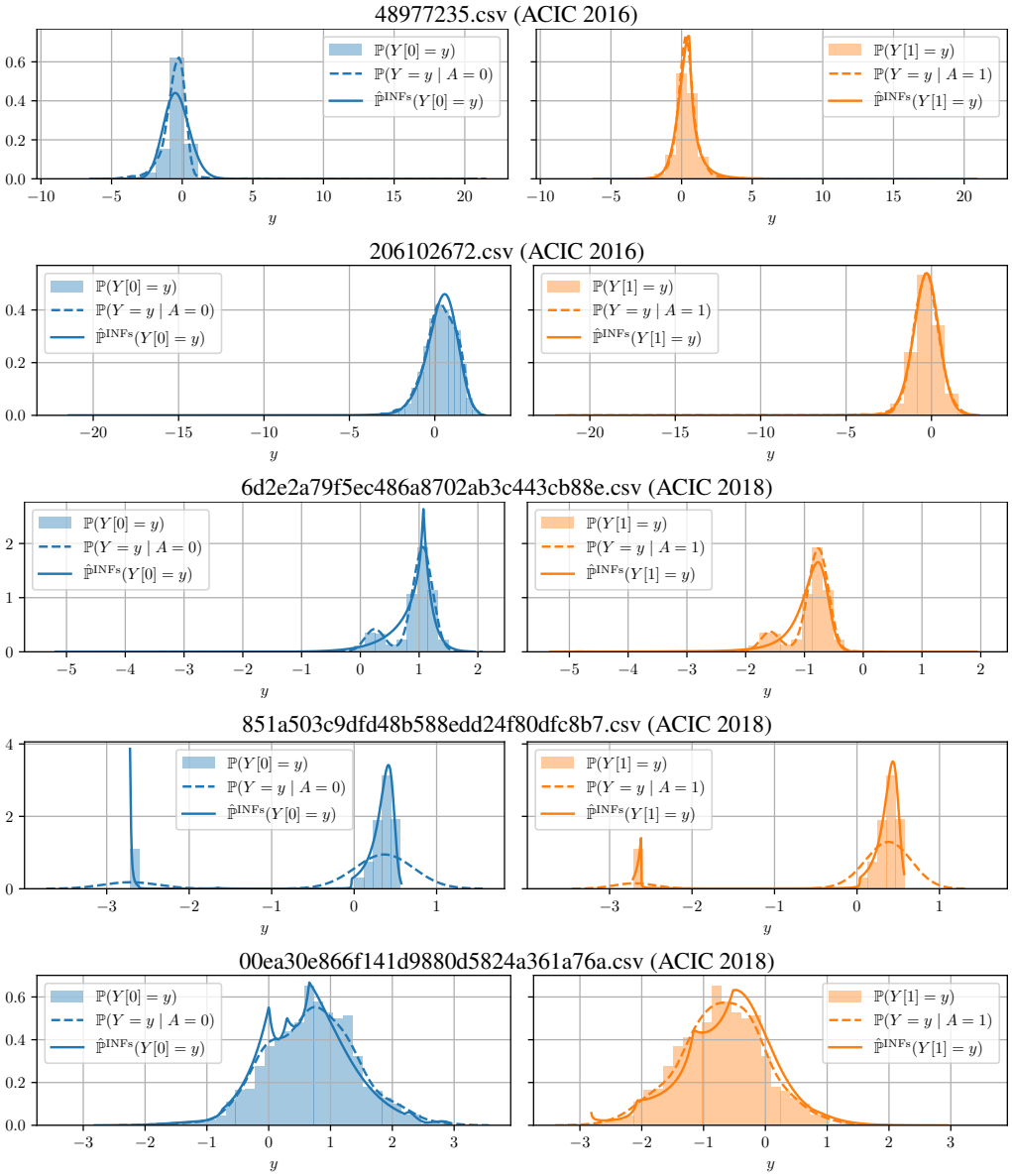

Figure 8. Examples of experiments where our INFs struggle to better understand their strengths and limitations. We picked five datasets from ACIC 2016 & 2018 where our INFs were inferior to the baselines (i.e., performing worst or second worst). In the plots, we show the empirical ground-truth interventional and conditional distributions of the outcomes. We also plot our INFs density estimator, i. e., $\hat{\mathbb{P}}^{\text{INFs}}(Y[a])$. Note that the x-axes range from the minimum to maximum observation in the dataset plus an offset.

L. Runtime comparison

INFs are a fully-parametric model and, therefore, provide a decent speed up at inference time. This is particularly important for scalability, that is, for datasets with large sample sizes and high-dimensional covariates. In Figure 9, we report the total runtime of the baselines and the different variants of our INFs together with a summary of the computational complexity. We see that the runtime of both full INFs and INFs w/o bias corr. stay relatively constant. In contrast to that, for the other baselines, the complexity grows polynomially with respect to the sample size. This demonstrates the benefits of our INFs in terms of scalability.

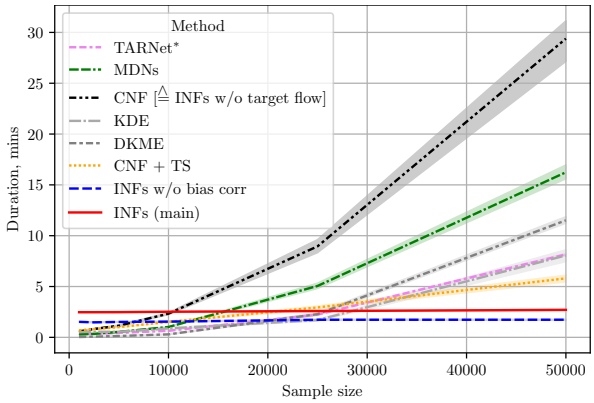

Method	Training time	Evaluation time
TARNet*, MDNs, CNF	$O(n_t \cdot d_X \cdot d_R)$	$O(n_t \cdot n_e \cdot d_R)$
KDE[a]	$O(n_t \cdot d_X \cdot d_R)$	$O(n_t \cdot n_e)$
DKME[b]	$O(n_t^2 \cdot (n_t + d_X))$	$O(n_t \cdot n_e)$
INFs, CNF+TS	$O(n_t \cdot d_X \cdot d_R)$	$O(n_e)$

n_t, n_e: sizes of train / evaluation subsets, respectively
d_R: size of representation
d_X: dimensionality of covariates
[a] with simplified variant of the functional regression, as in Appendix F
[b] complexity of matrix inversion is taken as $O(n_t^3)$

Figure 9. Total runtime (in minutes) of the experiments using ACIC 2018 datasets with different sample sizes (left) and computational for different models (right). Reported: mean $\pm$ standard deviation over four datasets and five runs for each size (lower is better). Experiments are carried out on Intel(R) Xeon(R) Silver 4316 CPU @ 2.30GHz.

M. Case study: California's tobacco control program

Overview. To show a real-world application of our INFs, we provide additional results using a case study where we evaluate the effect of California's tobacco control program (Abadie et al., 2010). This refers to the effect of Proposition 99, a large-scale tobacco control program introduced in California after 1988. Proposition 99 increased California's cigarette tax by 25 cents per pack, and earmarked the tax revenues to health and anti-smoking education. The main conclusion of Abadie et al. (2010) is that the effects of the tobacco control program are much larger than previously reported. The dataset has also found widespread use in causal inference ever since (e.g., Bellot & van der Schaar, 2021). In the original paper (Abadie et al., 2010), the results were based on a synthetic control method but without providing density estimates.

Dataset. After an initial preprocessing, the dataset consists of 39 states, including California. For each state, we observe several covariates (e. g., beer consumption per capita, GDP per capita, retail price, and percent of people aged 15–24) and the outcome, i. e., cigarette sales per capita. These are recorded annually for each year from 1970 to 2001. Further details on the datasets are in (Abadie et al., 2010).

To apply our INFs, we make several gross assumptions. First, as there is only one treated state, it is impossible to satisfy the positivity assumption. Therefore, we consider a tuple (state, year) as an independent unit of measurement, thus obtaining $n = 1209$ observations with 12 treated observations (i. e., those of the state of California after 1989). We also add a year as a covariate, which gives $d_X = 4 + 1$. We acknowledge that, even after the previous pre-processing, we still cannot formally guarantee the independence between units of measurement, as the observations of one state over time are not independent. Second, we assume the consistency holds, and there is no spillover effect between neighboring states so that the potential outcome of one state is independent of the others.

Results. We plot the empirical conditional and the estimated interventional distributions in Fig. 10. The results go in line with the conclusion in (Abadie et al., 2010). Our main finding is that the introduction of the Proposition 99 ($a = 1$) to all the states from 1970 would substantially reduce tobacco sales. In particular, the mass of the interventional density is shifted to the left which accounts for the reduction of the consumption.

As a robustness check, we analyze the role of the smoothness hyperparameter. Our conclusion remains consistent if one specifies different smoothness hyperparameter for the target flow, i. e. $n_{\text{knots,T}} = 5$ and 10. The specification of this hyperparameter is based on the prior knowledge of a researcher and cannot be chosen via observational data. However, we find consistent evidence of a positive effect.

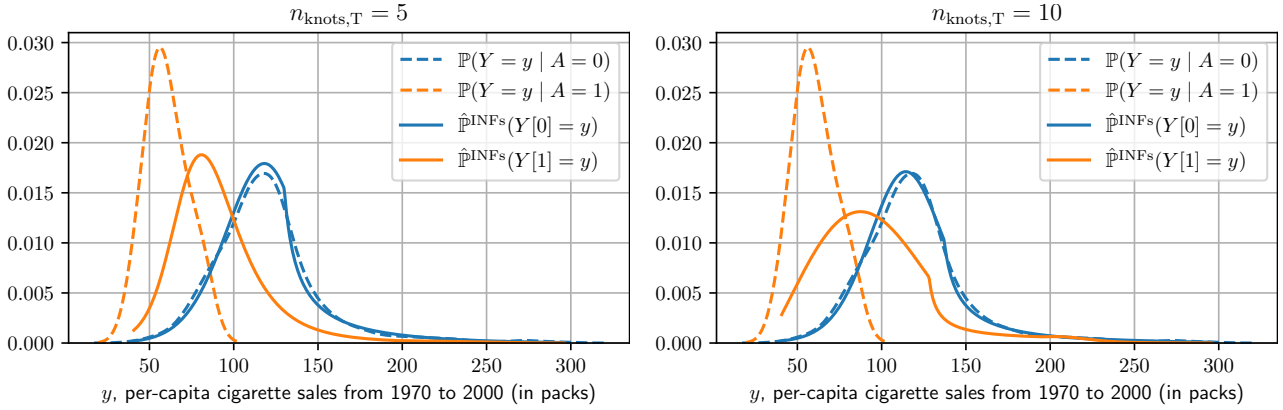

Figure 10. Empirical ground-truth conditional and estimated interventional distributions of cigarette sales per capita from 1970 to 2001. Treatment $a = 1$ corresponds to the introduction of the Proposition 99, that is, a comprehensive tobacco tax along with educational programs. We plot our INFs density estimator, $\hat{\mathbb{P}}^{\text{INFs}}(Y[a])$ with different smoothness hyperparameter values $n_{\text{knots,T}}$ of the target flow.